PHYSICAL REVIEW B **82**, 014521 (2010)

Competing order and nature of the pairing state in the iron pnictides

Rafael M. Fernandes* and Jörg Schmalian
Ames Laboratory and Department of Physics and Astronomy, Iowa State University, Ames, Iowa 50010, USA
(Received 13 May 2010; revised manuscript received 18 June 2010; published 16 July 2010)

We show that the competition between magnetism and superconductivity can be used to determine the pairing state in the iron arsenides. To this end we demonstrate that the itinerant antiferromagnetic (AFM) phase and the unconventional s^{+-} sign-changing superconducting (SC) state are near the borderline of microscopic coexistence and macroscopic phase separation, explaining the experimentally observed competition of both ordered states. In contrast, conventional s^{++} pairing is not able to coexist with magnetism. Expanding the microscopic free energy of the system with competing orders around the multicritical point, we find that static magnetism plays the role of an intrinsic interband Josephson coupling, making the phase diagram sensitive to the symmetry of the Cooper-pair wave function. We relate this result to the quasiparticle excitation spectrum and to the emergent SO(5) symmetry of systems with particle-hole symmetry. Our results rely on the assumption that the same electrons that form the ordered moment contribute to the superconducting condensate and that the system is close to particle-hole symmetry. We also compare the suppression of SC in different regions of the FeAs phase diagram, showing that while in the underdoped side it is due to the competition with AFM, in the overdoped side it is related to the disappearance of pockets from the Fermi surface.

DOI: 10.1103/PhysRevB.82.014521 PACS number(s): 74.20.Mn, 74.20.Rp, 74.25.Dw, 74.70.Xa

I. INTRODUCTION

The recent discovery of iron arsenide superconductors[1–4] brought renewed interest in the research of high-temperature superconductors. With transition temperatures T_c of more than 50 K in some cases, these compounds present a very rich phase diagram displaying superconducting (SC), antiferromagnetic (AFM), and structural order.[5–8] In some pnictides, such as $LaFeAs(O_{1-x}F_x)$, $PrFeAs(O_{1-x}F_x)$, $(Sr_{1-x}Na_x)Fe_2As_2$, and $(Ba_{1-x}K_x)Fe_2As_2$, the competing SC and AFM phases seem to be separated by a first-order transition and can only coexist in phase-separated macroscopic regions of the sample.[5,9–12] However, in other compounds, such as $Ba(Fe_{1-x}Co_x)_2As_2$ and possibly[6] $SmFeAs(O_{1-x}F_x)$, local probes[13–15] as well as bulk measurements[7,8,16–19] demonstrated that SC and AFM coexist homogeneously. This coexistence, however, is characterized by a competition of the two ordered states: neutron-diffraction experiments[18,19] revealed the dramatic suppression of the magnetization below T_c, to the extent that reentrance of the nonmagnetically ordered phase sets in at low temperatures.[20]

Experiments have also demonstrated the itinerant character of the magnetically ordered phase in the pnictides. In particular, optical conductivity measurements show a considerable Drude weight as well as a pronounced midinfrared peak below the Néel transition temperature T_N, consistent with the itinerant picture.[21,22] Furthermore, band-structure calculations reveal that the crystalline field is unable to significantly split the energy levels in order to localize $3d$ electrons.[23] Also, several theoretical models demonstrate the adequacy of the itinerant description.[24–27] Therefore, in the iron arsenides, the same electrons that form the superconducting condensate seem to be the ones that contribute to the ordered moment.

The interplay between AFM and SC has been investigated in many contexts,[28–37] including the pnictides.[20,38–43] In this paper, following results from our previous work[20] as well as from Refs. 41 and 42, we investigate in detail the connection between the competition of these two phases and the pairing symmetry of the SC state. We demonstrate that coexistence between SC and itinerant AFM in the pnictides for temperatures close to $T_N \simeq T_c$ is only possible if the pairing state is unconventional, as proposed by models with purely electronic pairing mechanisms.[44–52] In particular, using a mean-field Hamiltonian for the competition between AFM and SC and expanding the microscopic free energy in powers of the order parameters, we show that a conventional s^{++} SC state does not allow a coexistence regime to be established around the point where the T_N and T_c lines meet, even for extreme values of the band-structure parameters. Meanwhile, the unconventional s^{+-} state, whose gap function changes sign from one Fermi surface sheet to the other, may or may not coexist with AFM, depending on the details of the band-structure dispersion relations. Specifically, for the parameters of $Ba(Fe_{1-x}Co_x)_2As_2$, we find that the s^{+-} state coexists with itinerant AFM, while the s^{++} state does not (see Fig. 1).

Our results rely solely on the general assumptions that the magnetism is itinerant and that the band structure of the iron pnictides is not far from particle-hole symmetry, consisting of two distinct sets of Fermi-surface sheets:[53] hole pockets located at the center of the Brillouin zone and electron pockets displaced from the zone center by the magnetic ordering vector $\mathbf{Q}$. Additional details of the band structure, the dimensionality of the system, or the presence of intraband pairing interactions do not change the conclusions. On the other hand, for a localized AFM state, the free-energy expansion reveals that coexistence is easily attained, which is difficult to reconcile with the observation of phase separation in some compounds. Our analysis also indicates that the onset of SC has little effect on localized moments, which is at odds with experimental observations as well, giving further evidence for the itinerant magnetism in the pnictides.

We also investigate in detail the origin of the strong dependence of the phase diagram on the symmetry of the

 ©2010 The American Physical Society

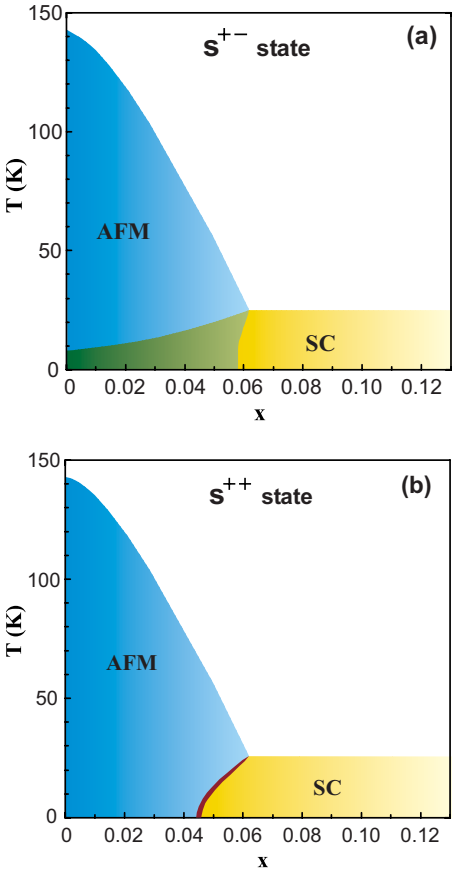

FIG. 1. (Color online) Phase diagrams of $Ba(Fe_{1-x}Co_x)_2As_2$ for a superconducting (a) s^{+-} state and an (b) s^{++} state, obtained by numerically solving the gap equations. The green region denotes homogeneous, microscopic coexistence, whereas the dark red region denotes heterogeneous, macroscopic coexistence. The band-structure parameters are discussed in Sec. IV B.

Cooper-pair wave function. Expressing the Ginzburg-Landau coefficients in terms of Feynman diagrams, it becomes clear that the static staggered magnetic moment **m** plays the role of an intrinsic interband Josephson coupling. Specifically, it corresponds to a term in the free energy of the form

$$E_J \propto \mathbf{m}^2|\Delta_1||\Delta_2|\cos\,\theta, \tag{1}$$

where θ is the relative phase between the SC order parameters of the two Fermi-surface sheets, Δ_1 and Δ_2. Thus, the coexistence state in some iron arsenides naturally carries information about the relative phase of the Cooper-pair wave functions, which are usually accessible only through intricate and delicate interference experiments.[54–56]

The quasiparticle excitation spectrum is substantially different for distinct pairing symmetries. For the special case of particle-hole symmetric bands, the system with competing magnetism and s^{++} pairing have two distinct positive eigenvalues $E_{\mathbf{k}}$ with $E_{\mathbf{k}}^2=\xi_{\mathbf{k}}^2+(M\pm\Delta)^2$, whereas for s^{+-} pairing the positive eigenvalues are degenerate: $E_{\mathbf{k}}^2=\xi_{\mathbf{k}}^2+M^2+\Delta^2$. We find that this special form of the excitation energy in the s^{+-} case implies that all quartic (and higher-order) Ginzburg-Landau terms must depend solely on the combination $(M^2+\Delta^2)$, which is the root of the SO(5) symmetry of the system and, ultimately, what leads to the conclusion that AFM and SC are in the borderline of coexistence and mutual exclusion. Inclusion of local moments add new terms to the free energy, removing the system from this borderline regime.

In this paper we also investigate some specific properties of the coexistence AFM-SC phase. We find that the effects of Coulomb repulsion on the magnetic superconducting phase are basically the same as in the case of a pure multiband superconductor. Particularly, the s^{+-} state is remarkably stable with respect to a uniform Coulomb repulsion. We also studied analytically the shape of the reentrant Néel transition line inside the SC state for low temperatures. At the mean-field level, the finite SC gap introduces an overall energy scale that causes the Néel line to have a divergent slope as $T\rightarrow 0$. Quantum fluctuations, which are relevant only in a very small region, end up suppressing the reentrant behavior.

The competition between AFM and SC explains the suppression of T_c in the underdoped side of the FeAs phase diagram. Here, we investigate the suppression of SC on the overdoped side as well. We find that the changes in the Fermi surface with doping are crucial to kill SC, in agreement to angle-resolved photoemission spectroscopy (ARPES) measurements.[57–59] In particular, the vanishing of one of the Fermi-surface pockets marks the onset of a regime where T_c is strongly suppressed with doping. In this regime, the s^{+-} state is fragile and easily destroyed by the Coulomb repulsion, contrasting to the situation where all Fermi pockets are present.

The paper is organized as follows: in Sec. II we discuss the competition between AFM and SC solely on phenomenological grounds. In Sec. III we introduce the mean-field Hamiltonian and derive the gap equations, the quasiparticle excitation spectrum, and the free-energy expansion. Section IV is devoted to the application of the formalism developed in Sec. III to the iron arsenides, and is divided in five subsections. In Sec. IV A, we present the results in the special case of a particle-hole symmetric band structure. Section IV B contains both analytical and numerical results for various band structures without particle-hole symmetry. Phase diagrams for parameters describing $Ba(Fe_{1-x}Co_x)_2As_2$ are presented. In Sec. IV C, we briefly discuss the regime where the sign of the coefficient that couples the AFM and SC order parameters becomes negative, and how it can be avoided by the onset of incommensurate AFM. Section IV D discusses the effects of intraband interactions and Coulomb repulsion. In Sec. IV E, we determine analytically the shape of the reentrant Néel transition line at low temperatures and the corrections due to fluctuations. In Sec. V we solve the same model presented in Sec. III but now with localized magnetic moments instead of itinerant AFM. Section VI discusses the suppression of T_c in the overdoped side of the pnictides phase diagram and how it is related to the doping evolution of the Fermi surface. Section VII is devoted to the conclusions and, in Appendix, we derive the Ginzburg-Landau coefficients in terms of Feynman diagrams. Some of the results have been published in a short publication.[20]

II. PHENOMENOLOGICAL ANALYSIS

Regardless of the microscopic details, the competition between superconductivity and antiferromagnetism near their

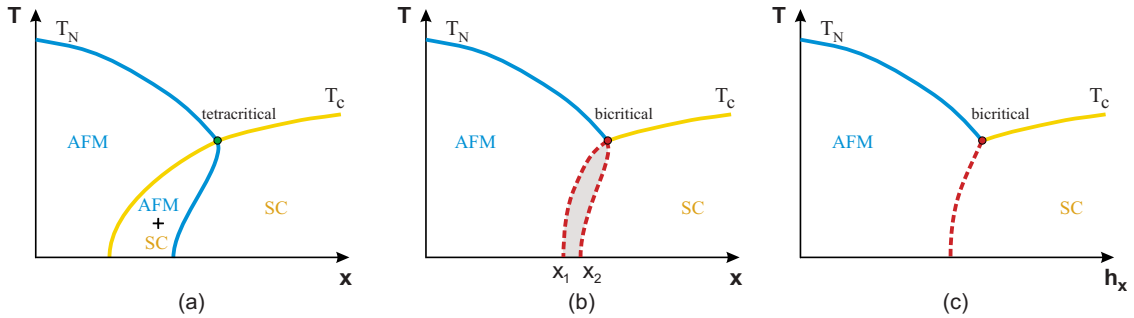

FIG. 2. (Color online) Schematic phase diagrams (x,T) for competing AFM and SC orders. Here, x is a generic physical parameter and T is the temperature. Solid (dashed) lines denote second-order (first-order) phase transitions. For $g<0$, there is a tetracritical point and a region of homogeneous coexistence (a), whereas for $g>0$ there is a bicritical point [(b) and (c)]. If x changes discontinuously across the first-order transition [panel (b)], forming a region of heterogeneous coexistence for $x_1<x<x_2$ (shaded area), then its conjugate variable h_x changes continuously and the phase diagram has only one first-order line [panel (c)].

finite-temperature phase transitions can be described in terms of a Ginzburg-Landau theory of coupled order parameters. The homogeneous part of the free energy is given as

$$F_{GL}(\Delta,\mathbf{M}) = \int d^d r\left(\frac{a_s}{2}|\Delta|^2 + \frac{u_s}{4}|\Delta|^4 + \frac{\gamma}{2}|\Delta|^2\mathbf{M}^2 + \frac{a_m}{2}\mathbf{M}^2 + \frac{u_m}{4}\mathbf{M}^4\right), \tag{2}$$

where Δ and $\mathbf{M}$ denote the SC and AFM order parameters, respectively. As usual, Δ is a complex order parameter, characterized by an amplitude and a phase, and $\mathbf{M}$ is a three component vector. The leading term in the order-parameter competition is characterized by the coefficient $\gamma>0$, where the sign of γ reflects that both ordered states compete. As usual, the quadratic coefficients are given by $a_m=a_{m,0}(T-T_{N,0})$ and $a_s=a_{s,0}(T-T_{c,0})$ and change sign at $T_{N,0}$ and $T_{c,0}$, denoting the Néel and SC transition temperatures without order-parameter competition. We consider the situation where the transitions for $\gamma=0$ are second order, i.e., the quartic coefficients u_m and u_s are positive.

Furthermore, we consider that $T_{N,0}(x)$ and $T_{c,0}(x)$ vary as function of a physical parameter x that could be pressure, electron density, or magnetic field. In case where both transitions meet at $x=x^*$, i.e., for

$$T^* \equiv T_{N,0}(x^*) = T_{c,0}(x^*), \tag{3}$$

we have a multicritical point (x^*,T^*) in the phase diagram. The vicinity of this multicritical point is the regime where a simultaneous expansion of the order parameters is allowed. The mean-field analysis of Eq. (2) allows for two options for the phase diagram near (x^*,T^*), depending if $\gamma^2>u_m u_s$ or $\gamma^2<u_m u_s$. Since we are interested in $\gamma>0$, it is convenient to define the dimensionless quantity[60]

$$g \equiv \frac{\gamma}{\sqrt{u_m u_s}} - 1. \tag{4}$$

Thus, the nature of the phase diagram is determined solely by the quartic coefficients in the Ginzburg-Landau expansion, Eq. (2). For $g<0$ (i.e., $0<\gamma<\sqrt{u_s u_m}$), (x^*,T^*) is a tetracritical point where two second-order phase lines cross, leading to a regime in the phase diagram where simultaneous AFM and SC order occurs homogeneously within the sample, see Fig. 2(a). In this regime both phases compete but do not exclude each other. On the other hand, if $g>0$ (i.e., $\gamma>\sqrt{u_s u_m}$) the phase competition is sufficiently strong that both phases are separated by a first-order transition that terminates at the bicritical point (x^*,T^*). Notice that if the parameter x jumps discontinuously from x_1 to x_2 at the first-order transition, there is an intermediate regime $x_1<x<x_2$ of heterogeneous phase coexistence, see Fig. 2(b). A sharp line of first-order transitions occurs if one considers the phase diagram as function of h_x, the variable that is thermodynamically conjugate to x, see Fig. 2(c). Critical fluctuations, that go beyond this mean-field analysis, change the universal exponents near the critical temperatures and the slopes of the phase lines near (x^*,T^*). However, neither the generic behavior shown in Fig. 1 nor the quantitative criterion based on the sign of g are changed by fluctuations.[61,62]

If we consider $g<0$, both order parameters can be finite simultaneously. This regime is often referred to as *coexistence* of AFM and SC, referring to coexistence of order. This should not be confused with phase coexistence in the thermodynamic sense. The area in Fig. 2(a) below the tetracritical point is a single thermodynamic phase characterized by two order parameters that are simultaneously finite. Similarly, the tetracritical point is not a point where four phases coexist (which would not be allowed by Gibbs phase rule) but a point where the system is in a single phase and both order parameters are infinitesimal simultaneously. Below the bicritical point, coexistence of thermodynamic phases only occurs for $x_1<x<x_2$, where macroscopic AFM and SC regions occur together in the sample. We use the term *homogeneous coexistence* of AFM and SC order below the tetracritical point to refer to coexisting order and *heterogeneous coexistence* below the bicritical point to refer to coexistence of phases.

From the Ginzburg-Landau expression, Eq. (2), we obtain the temperature dependence of the magnetic moment in the SC phase in the case of homogeneous coexistence,

$$\mathbf{M}^2(T) = \frac{a_{m,0}u_s(T_{N,0}-T) + a_{s,0}\gamma(T-T_{c,0})}{\sqrt{u_m u_s}-\gamma}. \tag{5}$$

Without phase competition both order parameters decrease as function of temperature, $d\mathbf{M}^2/dT<0$ and $d\Delta/dT<0$. Phase competition can change this behavior. For instance, if

$$a_{s,0}\gamma > a_{m,0}u_s, \tag{6}$$

it follows from Eq. (5) that $d\mathbf{M}^2/dT>0$ once superconductivity sets in. Thus, below T_c, the ordered moment decreases with decreasing temperature, as was observed in neutron-diffraction experiments[18,19] in both $Ba(Fe_{1-x}Co_x)_2As_2$ and[63] $Ba(Fe_{1-x}Rh_x)_2As_2$. It is interesting that the same condition implies a back bending of the antiferromagnetic phase boundary upon entering the superconducting state, see Fig. 1(a). To demonstrate this we write for the bare Néel temperature $T_{N,0}(x)=T_{c,0}[1+f(x)]$ with $df/dx<0$ and $f(x^*)=0$. Thus, $T_{N,0}$ is a monotonic decreasing function of x and meets the SC phase line at the carrier density or pressure value x^*. Without restriction we assume that $T_{c,0}$ is x independent near x^*. From the Ginzburg-Landau expansion, Eq. (2), follows that the Néel temperature T_N inside the SC phase is given by

$$T_N = T_{c,0}\left[1 - f(x)\frac{a_{m,0}u_s}{a_{s,0}\gamma - a_{m,0}u_s}\right]. \tag{7}$$

Since $df/dx<0$, it follows that $dT_N/dx>0$ in case Eq. (6) is valid. Thus close to x^* one finds reentrance of the paramagnetic phase below the SC transition temperature. In $Ba(Fe_{1-x}Co_x)_2As_2$ this was indeed observed.[18,19] The observation[63] of $d\mathbf{M}^2/dT>0$ in $Ba(Fe_{1-x}Rh_x)_2As_2$ implies that the phase line for this material must bend back as well. Furthermore, the SC transition temperature inside the AFM phase is given by

$$T_c = T_{c,0}\left[1 + f(x)\frac{a_{m,0}\gamma}{a_{m,0}\gamma - a_{s,0}u_m}\right]. \tag{8}$$

Using the condition Eq. (6) and the fact that $\gamma < \sqrt{u_m u_s}(g<0)$ it automatically holds that $a_{m,0}\gamma < a_{s,0}u_m$, implying $dT_c/dx>0$. Hence, the SC transition temperature is suppressed inside the AFM phase.

A very interesting limit is $g=0$, i.e., at the transition between the tetracritical point and bicritical point. Focusing on this multicritical point, where a_s and a_m change sign simultaneously, one can introduce the five-component vector,

$$\vec{\mathbf{N}} = \left(\frac{a_s}{a_m}\right)^{1/4}\left(\mathrm{Re}\,\Delta, \mathrm{Im}\,\Delta, \sqrt{\frac{a_m}{a_s}}\mathbf{M}\right). \tag{9}$$

In case where the additional condition $u_s=a_s^2u_m/a_m^2$ is fulfilled it follows that the free energy can be written as

$$F_{GL}(\Delta,\mathbf{M}) = \int d^dr\left(\frac{a}{2}\vec{\mathbf{N}}^2 + \frac{u}{4}\vec{\mathbf{N}}^4\right), \tag{10}$$

where $a=\mathrm{sign}(a_s)\sqrt{a_s a_m}$ and $u=\sqrt{u_s u_m}$. This is the SO(5) symmetric form of the Ginzburg-Landau energy that was first proposed by Zhang to describe the physics of the cuprate superconductors.[64,65] In the context of the pnictides, it was shown[66] that a model Hamiltonian similar to the one used in this paper is invariant with respect to a global SO(6) symmetry that contains, in addition to the AFM and SC order parameters, an imaginary density wave state. Below we will see that there is evidence that the pnictides are indeed strongly affected by such an enhanced symmetry.

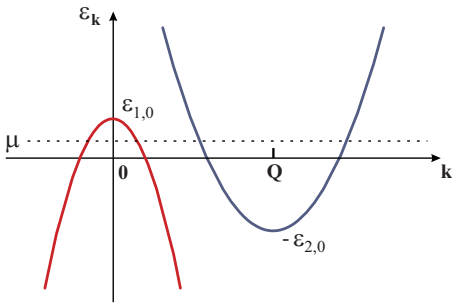

FIG. 3. (Color online) Schematic representation of the two-band structure used here. It consists of a circular hole band (band 1, red line) in the center of the Brillouin zone and an elliptical electron band (band 2, blue line) shifted by the ordering vector $\mathbf{Q}$ from the hole band. The chemical potential μ is positive for electron doping.

III. MICROSCOPIC MODEL

So far we have analyzed the problem of coexistence between SC and AFM only on phenomenological grounds, which gave us interesting and general information about the phase diagram. Next we develop a microscopic model that captures the essential aspects of the iron arsenides to determine their detailed phase diagram. We will also make explicit contact to the Ginzburg-Landau theory and determine the coefficients of the order-parameter expansion to obtain the behavior close to the transition temperatures.

We start from the Hamiltonian

$$\mathcal{H} = \mathcal{H}_0 + \mathcal{H}_{\mathrm{AFM}} + \mathcal{H}_{\mathrm{SC}}. \tag{11}$$

The noninteracting part $\mathcal{H}_0$ describes two bands shifted by the momentum $\mathbf{Q}$ relative to each other,

$$\mathcal{H}_0 = \sum_{\mathbf{k}\sigma}(\varepsilon_{1,\mathbf{k}} - \mu)c^\dagger_{\mathbf{k}\sigma}c_{\mathbf{k}\sigma} + \sum_{\mathbf{k}\sigma}(\varepsilon_{2,\mathbf{k}+\mathbf{Q}} - \mu)d^\dagger_{\mathbf{k}+\mathbf{Q}\sigma}d_{\mathbf{k}+\mathbf{Q}\sigma}. \tag{12}$$

We consider only one hole band located in the center of the Brillouin zone with dispersion $\varepsilon_{1,\mathbf{k}}$, and one electron band, shifted by $\mathbf{Q}$ from the hole band, with dispersion $\varepsilon_{2,\mathbf{k}}$. To keep the discussion as simple as possible, but still capturing the basic properties of these materials, we consider a circular hole band and an elliptical electron band,

$$\varepsilon_{1,\mathbf{k}} = \varepsilon_{1,0} - \frac{k^2}{2m},$$

$$\varepsilon_{2,\mathbf{k}+\mathbf{Q}} = -\varepsilon_{2,0} + \frac{k_x^2}{2m_x} + \frac{k_y^2}{2m_y}, \tag{13}$$

where $\varepsilon_{\alpha,0}$ is the energy offset (see Fig. 3). Such a choice is motivated by ARPES measurements (Ref. 53) as well as by tight-binding fittings to first-principles band-structure calculations. The operator $c^\dagger_{\mathbf{k}\sigma}$ ($d^\dagger_{\mathbf{k}+\mathbf{Q}\sigma}$) creates an electron with

momentum $\mathbf{k}(\mathbf{k}+Q)$ and spin σ in the hole (electron) band. The chemical potential is denoted by μ and we define $\xi_{\alpha,\mathbf{k}}=\varepsilon_{\alpha,\mathbf{k}}-\mu$. Frequently, it will be possible to gain explicit analytic insight by considering the limit of particle-hole symmetry, where $\varepsilon_0\equiv\varepsilon_{1,0}=\varepsilon_{2,0}$, $m_x=m_y=m$, and $\mu=0$. In this case the hole and electron Fermi surfaces are identical, leading to perfect nesting. In what follows we supplement our numerical analysis of the problem with the band structure of Eq. (13) by analytical results at or near the limit of particle-hole symmetry. Even though all five iron d orbitals contribute to the states at the Fermi surface of the iron arsenides, the physics of the competition between the antiferromagnetic and the superconducting states is well captured by this effective two-band model.[20]

The same electrons that form the Fermi surface are assumed to be responsible for the magnetism of the system through an electronic interband Coulomb interaction I, leading to excitonic itinerant antiferromagnetism,[26,67,68]

$$\mathcal{H}_{\mathrm{AFM}}=I\sum_{\mathbf{k},\mathbf{k}',\mathbf{q}}\sum_{s,s'}c^{\dagger}_{\mathbf{k}s}\boldsymbol{\sigma}_{ss'}d_{\mathbf{k}+\mathbf{q}s'}\cdot d^{\dagger}_{\mathbf{k}'s}\boldsymbol{\sigma}_{ss'}c_{\mathbf{k}'-\mathbf{q}s'}. \quad (14)$$

Here $\sigma^{(i)}_{ss'}$ denotes the (ss') element of the ith Pauli matrix with $s=\pm 1$. In the weak-coupling limit, we perform a Hartree-Fock decoupling that leads, except for a constant shift in energy, to the effective single-particle Hamiltonian

$$\mathcal{H}_{\mathrm{AFM}}=-\frac{1}{N}\sum_{\mathbf{k}s}sM(c^{\dagger}_{\mathbf{k}s}d_{\mathbf{k}+\mathbf{Q}s}+d^{\dagger}_{\mathbf{k}+\mathbf{Q}s}c_{\mathbf{k}s}), \quad (15)$$

where N is the system size. M denotes the antiferromagnetic gap opened at momenta $\mathbf{k}_0$ that are Bragg scattered due to magnetic order, $\xi_{1,\mathbf{k}_0}=\xi_{2,\mathbf{k}_0+\mathbf{Q}}$. In general, for small M, the Fermi surface is only partially gapped and the magnetic state is metallic. For large enough M, however, the Fermi surface can become completely gapped. In the case of perfect nested bands, an infinitesimal antiferromagnetic gap is already able to gap the entire Fermi surface. Note that $M=|\mathbf{M}|$ is proportional to the amplitude of the staggered magnetization $\mathbf{m}$ and given by

$$M=\frac{I}{2N}\sum_{\mathbf{k},s}s\langle c^{\dagger}_{\mathbf{k}s}d_{\mathbf{k}+\mathbf{Q}s}\rangle=Im. \quad (16)$$

Besides the magnetic interaction I, the electrons are also subject to a pairing interaction $V_{\alpha\beta}$, where $\alpha,\beta=1,2$ are band indices. In case of pure interband interaction $V_{\alpha\beta}=V(1-\delta_{\alpha\beta})$ the Hamiltonian becomes

$$\mathcal{H}_{\mathrm{SC}}=V\sum_{\mathbf{k},\mathbf{k}',\mathbf{q}}c^{\dagger}_{\mathbf{k}+\mathbf{q}\uparrow}c^{\dagger}_{-\mathbf{k}\downarrow}d_{-\mathbf{k}'-\mathbf{q}\uparrow}d_{\mathbf{k}'\uparrow}. \quad (17)$$

Below we demonstrate that the introduction of an intraband pairing interaction does not change the main conclusions of our paper. Δ_α is the superconducting gap of band α which, given the interband coupling V, is due to the action of the electrons in the opposite band $\bar{\alpha}$. Thus, Δ_1 and Δ_2 are determined by the two gap equations,

$$\Delta_2=-\frac{V}{N}\sum_{\mathbf{k}}\langle c^{\dagger}_{\mathbf{k}\uparrow}c^{\dagger}_{-\mathbf{k}\downarrow}\rangle,$$

$$\Delta_1=-\frac{V}{N}\sum_{\mathbf{k}}\langle d^{\dagger}_{\mathbf{k}+\mathbf{Q}\uparrow}d^{\dagger}_{-\mathbf{k}-\mathbf{Q}\downarrow}\rangle. \quad (18)$$

The expectation values are determined with the mean-field Hamiltonian,

$$\mathcal{H}_{\mathrm{SC}}=-\sum_{\mathbf{k}}(\Delta_1c^{\dagger}_{\mathbf{k}\uparrow}c^{\dagger}_{-\mathbf{k}\downarrow}+\mathrm{h.c.})-\sum_{\mathbf{k}}(\Delta_2d^{\dagger}_{\mathbf{k}+\mathbf{Q}\uparrow}d^{\dagger}_{-\mathbf{k}-\mathbf{Q}\downarrow}+\mathrm{h.c.}). \quad (19)$$

The mean-field Hamiltonian formed by the sum of Eqs. (12), (15), and (19) is quadratic and can be diagonalized analytically, yielding the self-consistent gap equations,

$$\Delta_\alpha=-\frac{V}{N}\sum_{\mathbf{k},a}K^{\Delta}_{\mathbf{k},\alpha}\tanh\left(\frac{\beta E_{a,\mathbf{k}}}{2}\right),$$

$$M=\frac{I}{N}\sum_{\mathbf{k},a}K^{M}_{\mathbf{k},\alpha}\tanh\left(\frac{\beta E_{a,\mathbf{k}}}{2}\right) \quad (20)$$

with kernels

$$K^{\Delta}_{\mathbf{k},\alpha}=\frac{\Delta_{\bar{\alpha}}(E^2_{a,\mathbf{k}}-\Delta^2_\alpha-\xi^2_{\alpha,\mathbf{k}})+M^2\Delta_\alpha}{2E_{a,\mathbf{k}}(E^2_{a,\mathbf{k}}-E^2_{\bar{a},\mathbf{k}})},$$

$$K^{M}_{\mathbf{k},\alpha}=\frac{M(E^2_{a,\mathbf{k}}+\Delta_1\Delta_2+\xi_{1,\mathbf{k}}\xi_{2,\mathbf{k}}-M^2)}{2E_{a,\mathbf{k}}(E^2_{a,\mathbf{k}}-E^2_{\bar{a},\mathbf{k}})}. \quad (21)$$

The excitation energies $E_{a,\mathbf{k}}$ $(a=1,2)$ are the positive eigenvalues of a state with simultaneous magnetic and superconducting order,

$$E^2_{a,\mathbf{k}}=\frac{1}{2}(\Gamma_{\mathbf{k}}\pm\sqrt{\Gamma^2_{\mathbf{k}}+\Omega_{\mathbf{k}}+\delta_{\mathbf{k}}}) \quad (22)$$

with $\Gamma_{\mathbf{k}}=2M^2+\Delta_1^2+\Delta_2^2+\varepsilon^2_{\mathbf{k},1}+\varepsilon^2_{\mathbf{k}+\mathbf{Q},2}$ and $\Omega_{\mathbf{k}}=-4(\varepsilon^2_{\mathbf{k},1}+\Delta_1^2)(\varepsilon^2_{\mathbf{k}+\mathbf{Q},2}+\Delta_2^2)$ as well as $\delta_{\mathbf{k}}=8M^2(\Delta_1\Delta_2+\varepsilon_{\mathbf{k},1}\varepsilon_{\mathbf{k}+\mathbf{Q},2}-M^2/2)$. The free-energy density of a system with SC and AFM long-range order that results from this analysis is

$$f(M,\Delta_\alpha)=\frac{2}{I}M^2-\frac{1}{V}(\Delta_1^*\Delta_2+\Delta_2^*\Delta_1)-\frac{2T}{N}\sum_{\mathbf{k},a}\log\left[2\cosh\left(\frac{E_{a,\mathbf{k}}}{2k_BT}\right)\right]. \quad (23)$$

The superconducting order parameters Δ_1 and Δ_2 of the two bands and the staggered moment $\propto M$ are obtained by minimizing $f(M,\Delta_\alpha)$. The gap equations [Eq. (20)] follow as the stationary points $\partial f(M,\Delta_\alpha)/\partial\Delta_\alpha=\partial f(M,\Delta_\alpha)/\partial M=0$.

Before we analyze the impact of magnetic long-range order on the pairing state we discuss the gap equations [Eq. (20)] in the limit $M=0$. Here, we perform the momentum integration by introducing the density of states ρ_1 and ρ_2 of the two bands. The condition for T_c is that the largest eigenvalue of

$$\Lambda = \begin{pmatrix} 0 & -V\rho_2 \\ -V\rho_1 & 0 \end{pmatrix} \tag{24}$$

is positive and equals to $1/\ln[W/(\alpha T_c)]$, were $\alpha = \pi e^{-\gamma_E}/2$, γ_E is Euler's constant and W is an upper energy cutoff for the pairing interaction. Clearly, the eigenvalues of Λ are $\lambda_\pm = \pm V\sqrt{\rho_1\rho_2}$. The pairing state is determined by the corresponding eigenvector,

$$(\Delta_1, \Delta_2) \propto \frac{1}{\sqrt{\rho_1 + \rho_2}}(\sqrt{\rho_2}, \mp\sqrt{\rho_1}). \tag{25}$$

Thus, for $V<0$, λ_- is the largest eigenvalue and the gap equation has a solution where Δ_1 and Δ_2 on the two sheets of the Fermi surface have the same sign. This is called the s^{++} state and is analogous to the pairing state of the multiband superconductor[69] MgB_2. It is the natural state that arises as a result of conventional electron-phonon interactions. On the other hand, the gap equations also allow for a solution for $V>0$ with Δ_1 and Δ_2 having different signs on distinct Fermi-surface sheets. This s^{+-}-state results from purely electronic interactions,[24,44–46,48–52] i.e., it is the natural analog to the $d_{x^2-y^2}$-pairing state in the cuprates with a single Fermi-surface sheet. As the relative sign of Δ_1 and Δ_2 is -1, this is an unconventional SC state, even though it is in the same irreducible representation A_{1g} of the symmetry group D_{4h} as the s^{++} state.

In case where Δ_1 and Δ_2 have the same sign (s^{++} state), the excitation energies $\pm E_{2,\mathbf{k}}$ possibly have nodes.[40] The nodes are located at the set of points $\mathbf{k}_n$ that satisfy simultaneously the equations,

$$\xi_{1,\mathbf{k}_n} = \pm\sqrt{\frac{\Delta_1}{\Delta_2}}(M^2 - \Delta_1\Delta_2)^{1/2},$$

$$\xi_{2,\mathbf{k}_n+\mathbf{Q}} = \pm\sqrt{\frac{\Delta_2}{\Delta_1}}(M^2 - \Delta_1\Delta_2)^{1/2} \tag{26}$$

determined from the condition $E_{2,\mathbf{k}}=0$. Obviously, one condition for nodes to exist is $M^2 \geq \Delta_1\Delta_2$. For $\Delta_1=\Delta_2$ the condition for nodes in the antiferromagnetic state corresponds to $\xi_{1,\mathbf{k}_n} = \xi_{2,\mathbf{k}_n+\mathbf{Q}}$, i.e., where Bragg scattering due to antiferromagnetism is large. However, nodes are not guaranteed to emerge. For example, in the case of particle-hole symmetry (implying perfect nesting of the Fermi surface)

$$\xi_{\mathbf{k}} \equiv \xi_{1,\mathbf{k}} = -\xi_{2,\mathbf{k}+\mathbf{Q}}, \tag{27}$$

it holds for $I>|V|$ that $\Delta \equiv \Delta_1 = \pm\Delta_2 = \frac{|V|}{I}M < M$ and the above equations cannot be fulfilled simultaneously. This also follows if one explicitly considers the eigenvalues for s^{++} pairing in the limit of particle-hole symmetry,

$$E^2_{a,\mathbf{k}} = \xi^2_{\mathbf{k}} + (M \pm \Delta)^2, \tag{28}$$

which are fully gapped for $M \neq \Delta$. Only for $|V|=I$ follows an entirely gapless eigenvalue $E_{2,\mathbf{k}}$, consistent with the condition given by Eq. (26). In distinction, the eigenvalues for s^{+-} pairing and particle-hole symmetry are fully gapped and doubly degenerate,

$$E^2_{a,\mathbf{k}} = \xi^2_{\mathbf{k}} + M^2 + \Delta^2. \tag{29}$$

It is also interesting to note that, if one considers the simplification $\Delta=\Delta_1=-\Delta_2$ even in the absence of particle-hole symmetry, then the excitation energies for the s^{+-} case assume the simple form $E^2_{a,\mathbf{k}} = (E^{\mathrm{AFM}}_{a,\mathbf{k}})^2 + \Delta^2$, where

$$E^{\mathrm{AFM}}_{a,\mathbf{k}} = \left(\frac{\xi_{1,\mathbf{k}} + \xi_{2,\mathbf{k}}}{2}\right) \pm \sqrt{M^2 + \left(\frac{\xi_{1,\mathbf{k}} - \xi_{2,\mathbf{k}}}{2}\right)^2} \tag{30}$$

are the excitation energies of the pure AFM state. Thus, in this special situation, one can perform two separate Bogolyubov transformations to diagonalize the full Hamiltonian.

These considerations allow for some general conclusions of the order-parameter dependence of the free energy, Eq. (23). The quadratic terms of $f(M, \Delta_\alpha)$ depend on the interaction strengths I and $|V|$. However, all other dependencies take place only via the implicit dependence of $E_{a,\mathbf{k}}$ on the order parameters. In case of s^{++} pairing, the order parameters enter these extra dependencies through the combinations $(M \pm \Delta)^2$, while for s^{+-} pairing the third term in Eq. (23) can only depend on the combination $M^2+\Delta^2$. Thus, we find for the free energy of the s^{+-} state with particle-hole symmetry,

$$f_{+-} = \frac{2M^2}{I} + \frac{2\Delta^2}{|V|} + 2\Phi(M^2 + |\Delta|^2). \tag{31}$$

On the other hand, it follows for the s^{++} state,

$$f_{++}(\Delta, M^2) = \frac{2M^2}{I} + \frac{2\Delta^2}{|V|} + \Phi[(|M| + |\Delta|)^2] + \Phi[(|M| - |\Delta|)^2], \tag{32}$$

where

$$\Phi(x) = -4T\rho\int_{|x|}^{\infty} dz \frac{z\log[2\cosh(\beta z/2)]}{\sqrt{z^2 - x^2}} \tag{33}$$

is the same function in both cases. These facts have important implications for the Landau expansion of the free energy that we discuss next.

In order to obtain microscopic expressions for the coefficients of the Ginzburg-Landau theory, we expand $\delta f(\mathbf{M}, \Delta_\alpha) = f(\mathbf{M}, \Delta_\alpha) - f(0,0)$ with respect to $\mathbf{M}$ and Δ_α. It follows from Eq. (23) that

$$\delta f = \frac{a_m}{2}\mathbf{M}^2 + \frac{u_m}{4}\mathbf{M}^4 + \sum_{\alpha,\beta}\frac{a_{s,\alpha\beta}}{2}\Delta_\alpha\Delta_\beta + \sum_\alpha \frac{u_{s,\alpha}}{4}\Delta^4_\alpha + \sum_{\alpha,\beta}\frac{\gamma_{\alpha\beta}}{2}\mathbf{M}^2\Delta_\alpha\Delta_\beta. \tag{34}$$

For the coefficients of the antiferromagnetic order parameter follows

$$a_m = \frac{4}{I} - 2\chi_{ph}(\mathbf{Q}),$$

$$u_m = \frac{1}{N}\sum_{\mathbf{k}} \frac{A_{1,\mathbf{k}}\,\mathrm{sech}^2\left(\frac{\xi_{1,\mathbf{k}}}{2T}\right) - A_{2,\mathbf{k}+\mathbf{Q}}\,\mathrm{sech}^2\left(\frac{\xi_{2,\mathbf{k}+\mathbf{Q}}}{2T}\right)}{T(\xi_{1,\mathbf{k}} - \xi_{2,\mathbf{k}+\mathbf{Q}})^3} \tag{35}$$

with coefficients $A_{\alpha,\mathbf{k}} = -\xi_{\alpha,\mathbf{k}} + \xi_{\bar{\alpha},\mathbf{k}+\mathbf{Q}} + 2T\sinh(\xi_{\alpha,\mathbf{k}}/T)$ and the bare static particle-hole response at the antiferromagnetic ordering vector,

$$\chi_{ph}(\mathbf{Q}) = \frac{1}{N}\sum_{\mathbf{k}} \frac{\tanh\left(\frac{\xi_{1,\mathbf{k}}}{2T}\right) - \tanh\left(\frac{\xi_{2,\mathbf{k}+\mathbf{Q}}}{2T}\right)}{\xi_{1,\mathbf{k}} - \xi_{2,\mathbf{k}+\mathbf{Q}}}. \tag{36}$$

For the coefficients of the superconducting order parameters follows

$$a_{s,\alpha\beta} = -\frac{2}{V}(1-\delta_{\alpha\beta}) - \delta_{\alpha\beta}\chi_{pp}(\mathbf{0}),$$

$$u_{s,\alpha} = \frac{1}{4NT}\sum_{\mathbf{k}} \frac{\mathrm{sech}^2\left(\frac{\xi_{\alpha,\mathbf{k}}}{2T}\right)[T\sinh(\beta\xi_{\alpha,\mathbf{k}}) - \xi_{\alpha,\mathbf{k}}]}{\xi_{\alpha,\mathbf{k}}^3}, \tag{37}$$

where

$$\chi_{pp}(\mathbf{0}) = \frac{1}{N}\sum_{\mathbf{k},\alpha} \frac{\tanh\left(\frac{\xi_{\alpha,\mathbf{k}}}{2T}\right)}{\xi_{\alpha,\mathbf{k}}} \tag{38}$$

is the bare static particle-particle response at external momentum $\mathbf{q}=\mathbf{0}$. Finally, it follows for the coefficients $\gamma_{\alpha\beta}$ that determine the coupling between both order parameters,

$$\gamma_{\alpha\alpha} = \frac{1}{2N}\sum_{\mathbf{k},i=1}^{3} \frac{C_{\alpha,\mathbf{k}}^{(i)}}{T\xi_{\alpha,\mathbf{k}}^2(\xi_{\alpha,\mathbf{k}} + \xi_{\bar{\alpha},\mathbf{k}})(\xi_{\alpha,\mathbf{k}} - \xi_{\bar{\alpha},\mathbf{k}})^2},$$

$$\gamma_{\alpha\bar{\alpha}} = \frac{1}{N}\sum_{\mathbf{k}} \frac{\xi_{\alpha,\mathbf{k}}\tanh(\beta\xi_{\bar{\alpha},\mathbf{k}}/2) - \xi_{\bar{\alpha},\mathbf{k}}\tanh(\beta\xi_{\alpha,\mathbf{k}}/2)}{T\xi_{\alpha,\mathbf{k}}\xi_{\bar{\alpha},\mathbf{k}}(\xi_{\alpha,\mathbf{k}}^2 - \xi_{\bar{\alpha},\mathbf{k}}^2)} \tag{39}$$

with $C_{\alpha,\mathbf{k}}^{(1)} = 2T\tanh(\beta\xi_{\alpha,\mathbf{k}}/2)(\xi_{\alpha,\mathbf{k}}^2 - \xi_{\bar{\alpha},\mathbf{k}}^2 + 2\xi_{\alpha,\mathbf{k}}\xi_{\bar{\alpha},\mathbf{k}})$, $C_{\alpha,\mathbf{k}}^{(2)} = -\xi_{\alpha,\mathbf{k}}(\xi_{\alpha,\mathbf{k}}^2 - \xi_{\bar{\alpha},\mathbf{k}}^2)\mathrm{sech}^2(\beta\xi_{\alpha,\mathbf{k}}/2)$ as well as $C_{\alpha,\mathbf{k}}^{(3)} = -4T\xi_{\alpha,\mathbf{k}}^2\tanh(\beta\xi_{\bar{\alpha},\mathbf{k}}/2)$.

These Ginzburg-Landau coefficients can also be expressed in terms of Feynman diagrams obtained by integrating out the fermionic degrees of freedom of the system with competing AFM and SC. The derivation is presented in Appendix; in Fig. 4, we show the diagrammatic representation of all the quartic coefficients in terms of the single-particle Green's function $G_i(k) = (i\omega_n - \xi_{i,\mathbf{k}})^{-1}$.

Due to the coupling between the two bands, Δ_1 and Δ_2 will always appear simultaneously. As follows from the eigenvectors of Λ in Eq. (24), close to T_c, the ratio $\Delta_1/\Delta_2 = \pm(\rho_2/\rho_1)^{1/2}$ is determined by the ratio between the densities of states of the two bands. In our case holds $\rho_2/\rho_1 = \sqrt{m_x m_y}/m$. The relative sign of Δ_1 and Δ_2 depends on the sign of V. Thus, one can introduce the superconducting order parameter Δ via

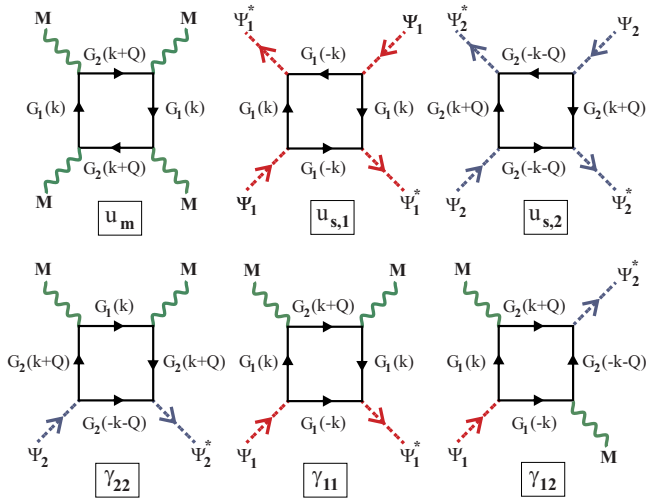

FIG. 4. (Color online) Diagrammatic representation of the quartic Ginzburg-Landau coefficients associated to the system with competing AFM and SC order parameters. The single-particle Green's function of the two bands are denoted by $G_i(k)$.

$$\Delta_1 = \sqrt{\frac{2\rho_2}{\rho_1+\rho_2}}\Delta,$$

$$\Delta_2 = \pm\sqrt{\frac{2\rho_1}{\rho_1+\rho_2}}\Delta \tag{40}$$

such that $\Delta^2 = (\Delta_1^2 + \Delta_2^2)/2$. This leads to the Landau expansion coefficients of the superconducting order parameter of Eq. (2),

$$a_s = \frac{2a_{s,11}\rho_2 + 2a_{s,22}\rho_1 + 4|a_{s,12}|\sqrt{\rho_1\rho_2}}{(\rho_1+\rho_2)},$$

$$u_s = \frac{4u_{s,1}\rho_2^2 + 4u_{s,2}\rho_2^2}{(\rho_1+\rho_2)^2},$$

$$\gamma = \frac{2\gamma_{11}\rho_2 + 2\gamma_{22}\rho_1 \pm 4\gamma_{12}\sqrt{\rho_1\rho_2}}{(\rho_1+\rho_2)}. \tag{41}$$

Note that the coefficient γ of the coupling between the SC and AFM order parameters depends on the relative phase of the two SC order parameters. In the next section we analyze these expressions and discuss the implications of these results for the phase diagram of the pnictides.

Before moving on, let us briefly discuss the relationship between the system's dimensionality and the Néel transition temperature. Since our mean-field model is insensitive to fluctuations, it allows a finite T_N even for two dimensions. However, due to Hohenberg-Mermin-Wagner theorem,[70] a nonzero T_N will only be possible if the band structure has a three-dimensional (3D) dispersion, i.e., if the electronic interaction responsible for the AFM instability is effectively 3D. In the iron arsenides, the AFM ordering involves Fe ions

located on spatially separated layers. Assuming a weak interlayer coupling, we can introduce a phenomenological 3D anisotropic action for the low-energy collective magnetic modes and obtain the Néel transition temperature T_N,

$$\frac{T_N - T_N^0}{T_N} \simeq \ln\left(\frac{J_z}{J}\right). \tag{42}$$

Here, J is the effective in-plane magnetic exchange, J_z is the interlayer coupling, and T_N^0 is the mean-field Néel transition temperature. Notice that J and J_z are effective parameters of the low-energy model originated by the electronic interaction, Eq. (14), and are not necessarily related to localized spins. The logarithmic dependence of T_N on J_z/J shows that the overall scale of the transition temperature of an anisotropic magnetic material is determined by the mean-field value T_N^0. This explains why, in the iron arsenides, T_N has the same order of magnitude for both the 1111 and the 122 compounds, even though the former are much more anisotropic than the latter.

IV. PHASE DIAGRAMS

In this section, we will use the formalism developed above to explore the possible phase diagrams of the system with competing SC and AFM order. In particular, we will be interested in analyzing whether different superconducting states are able to coexist with an itinerant antiferromagnetic state or destined to phase separate from it.

A. Particle-hole symmetric case

As we stated in Sec. III, the band structure of the iron arsenides can be generically described by two sets of hole and electron bands, displaced from each other by the magnetic ordering vector $\mathbf{Q}$. Even though the electron and hole bands are not perfectly symmetric to each other, we can start our analysis by considering, at first, the case of two nested bands, such that $\xi_{\mathbf{k}} \equiv \xi_{1,\mathbf{k}} = -\xi_{2,\mathbf{k}+\mathbf{Q}}$. Notice that, in this context, nesting does not mean that the distinct pockets of the Fermi surface have parallel segments; instead, it implies that they have the same shape and area, such that the noninteracting Hamiltonian $\mathcal{H}_0$ has particle-hole symmetry.

The limit of perfect nesting corresponds to $\varepsilon_0 \equiv \varepsilon_{1,0} = \varepsilon_{2,0}$, $m_x = m_y = m$, and $\mu = 0$ in Eq. (13). In this case, it is straightforward to conclude that $\Delta = |\Delta_1| = |\Delta_2|$. Moreover, using formula (37), it follows that $a_{s,11} = a_{s,22}$ and $u_{s,1} = u_{s,2}$. Thus, independently of the relative sign between the Cooper-pair wave functions of the two bands, they have the same SC Ginzburg-Landau coefficients, meaning that the thermodynamic properties of the "pure" s^{++} and s^{+-} states will be the same. However, the coupling to the magnetic degrees of freedom significantly changes this picture.

The Ginzburg-Landau expansion is formally valid around the temperature where the AFM and SC phase lines meet, $T_N \simeq T_c$. From the magnetic and superconducting quadratic coefficients, we see that, for particle-hole symmetry, this condition implies $I = |V|$. Thus, calculation of the Ginzburg-Landau coefficients using Eqs. (35), (37), and (39) yields

$$a \equiv a_m = a_s = \frac{4}{I} - \frac{2}{N}\sum_{\mathbf{k}} \frac{\tanh\left(\frac{\xi_{\mathbf{k}}}{2T}\right)}{\xi_{\mathbf{k}}} = 4\left[\frac{1}{I} - \rho \ln\left(\frac{W}{\alpha T}\right)\right], \tag{43}$$

where $\alpha = \pi e^{-\gamma_E}/2$ as well as

$$u \equiv u_m = u_s = \gamma_{11} = \gamma_{22} = 2\gamma_{12} \tag{44}$$

with

$$u = \frac{1}{2NT}\sum_{\mathbf{k}} \frac{\mathrm{sech}^2\left(\frac{\xi_{\mathbf{k}}}{2T}\right)\left[T \sinh\left(\frac{\xi_{\mathbf{k}}}{T}\right) - \xi_{\mathbf{k}}\right]}{\xi_{\mathbf{k}}^3} = \frac{\rho}{T_c^2}\frac{7\zeta(3)}{2\pi^2}. \tag{45}$$

Inserting these results into the Ginzburg-Landau expansion, Eq. (34), yields[20]

$$\delta f(\mathbf{M}, \Delta) = \frac{a}{2}(\mathbf{M}^2 + \Delta^2) + \frac{u}{4}(\mathbf{M}^2 + \Delta^2)^2 + g\frac{u}{2}\mathbf{M}^2\Delta^2, \tag{46}$$

where $g = (1 + \cos\theta)$, as given by Eq. (4), with θ denoting the relative phase between the SC order parameters of the electron and hole bands. Thus, for the s^{++} state ($\theta = 0$), it follows that $g = 2 > 0$, meaning that the s^{++} state is deep in the mutual exclusion regime, unable to coexist with AFM in the region of the phase diagram close to $T_N \simeq T_c$. However, for the s^{+-} state it holds that $g = 0$, implying that this state is in the borderline between the coexistence and mutual exclusion regimes.

We can trace back to the Ginzburg-Landau coefficients in Eqs. (35), (37), and (39) the origin for the distinct behaviors of the systems with competing itinerant antiferromagnetism and s^{++} or s^{+-} superconductivity. As we showed above, the quadratic and quartic SC and AFM coefficients are the same in both cases. However, the net SC-AFM coupling coefficient $\gamma_{+-} = \gamma_{11} + \gamma_{22} - 2\gamma_{12}$ is reduced in the case of an s^{+-} state when compared to the case of an s^{++} state, where $\gamma_{++} = \gamma_{11} + \gamma_{22} + 2\gamma_{12}$. Notice that in both situations $\gamma > 0$, evidencing the competition between the two phases.

In fact, from the diagrammatic representation of the coefficients presented in Fig. 4, it is clear that the only Feynman diagram sensitive to the relative phase between the SC order parameters of the two bands is the diagram corresponding to γ_{12}. It gives a contribution to the free energy of the form $M^2|\Delta_1||\Delta_2|\cos\theta$, see Eq. (1). Therefore, the static long-range magnetic order plays the role of an intrinsic Josephson coupling: it provides the momentum $\mathbf{Q}$ to the electrons of a Cooper pair in band 1, scattering them coherently to band 2, where they recombine. Thus, the region of the phase diagram where antiferromagnetism and superconductivity compete provides an efficient tool to probe the relative phase between the Cooper-pair wave functions, an information that is usually reserved to very delicate phase sensitive experiments.[54–56] The existence of such a tool is even more relevant in the case of the iron arsenides, since both s^{++} and s^{+-} states belong to the same irreducible representation A_{1g}

of the tetragonal point group D_{4h}, making interference experiments rather involved and complex.[56,71–73]

The analysis of this limiting case with particle-hole symmetry suggests that while the s^{++} state is intrinsically unsuitable for coexistence with the AFM phase in the iron arsenides, the s^{+-} state may or may not coexist with magnetism. In the realistic case where particle-hole symmetry does not hold, the decision on whether the s^{+-} state is in the regime of coexistence or mutual exclusion will depend on additional details of the band structure, as we will demonstrate in Sec. IV B. This explains why some compounds present homogeneous coexistence,[7,8,13–19] such as $Ba(Fe_{1-x}Co_x)_2As_2$ and possibly[6] $SmFeAs(O_{1-x}F_x)$, while in others, such as $LaFeAs(O_{1-x}F_x)$, $PrFeAs(O_{1-x}F_x)$, $(Sr_{1-x}Na_x)Fe_2As_2$, and $(Ba_{1-x}K_x)Fe_2As_2$, AFM and SC are mutually excluding.[5,9–12]

Notice that these results do not depend on the specific functional form of the bands dispersion relations nor on the dimensionality of the system. They follow solely from the assumption of particle-hole symmetry $\xi_{1,\mathbf{k}}=-\xi_{2,\mathbf{k}+\mathbf{Q}}$. Note also that, as we anticipated in the previous sections, the free energy, Eq. (46), for the s^{+-} case is completely symmetric with respect to both order parameters and can be characterized by the SO(5) order parameter $\vec{\mathbf{N}}=(\mathrm{Re}\,\Delta,\mathrm{Im}\,\Delta,\mathbf{M})$. Remarkably, a similar SO(5) model has been proposed previously for the cuprates.[64,65] In the context of the iron arsenides, recent works[66,74] demonstrated that the complete, interacting particle-hole symmetric Hamiltonian has an emergent SO(6) symmetry (the other degree of freedom which is not captured in our model is associated to an imaginary density wave). The existence of such an emergent symmetry suggests that our result regarding the ability of the s^{+-} state to coexist with magnetism is likely valid not only in our weak-coupling approach but also in the strong-coupling limit.

B. General case and application to $Ba(Fe_{1-x}Co_x)_2As_2$

We now move away from the particle-hole symmetric case and consider more specific details of the band-structure dispersions of the iron arsenides. Let us first consider small perturbations that break the particle-hole symmetry. For instance, we first take $\varepsilon_0\equiv\varepsilon_{1,0}=\varepsilon_{2,0}$, $m_x=m_y=m$ but a finite chemical potential $\mu\ll T$, i.e., we have two detuned circular bands. An analytic expansion yields, to leading order

$$g_{+-}\approx 0.018\left(\frac{\mu}{T}\right)^4,$$

$$g_{++}\approx 2+0.386\left(\frac{\mu}{T}\right)^2. \tag{47}$$

Thus, in the case of spherical detuned bands, we always find a first-order transition between the superconducting and magnetic phases, independent of the pairing state. This is in agreement with numerical calculations performed by Vorontsov *et al.*,[38] which found no region of coexistence between commensurate AFM and SC.

The second perturbation we consider is an infinitesimal ellipticity of the electron band, such that $m_x=m+\delta m$ and $m_y=m-\delta m$, but with $\varepsilon_0\equiv\varepsilon_{1,0}=\varepsilon_{2,0}$ and $\mu=0$. Such perturbation also makes $|\Delta_1|$ and $|\Delta_2|$ assume different values. In this case, we obtain the following perturbative expansion of g for the s^{+-} case

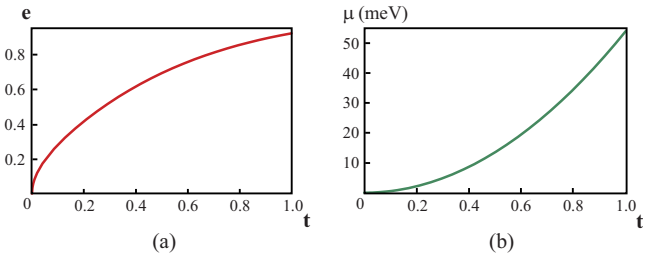

FIG. 5. (Color online) (a) Ellipticity of the electron band $e=\sqrt{1-\frac{m_y}{m_x}}$ and (b) chemical potential μ (in meV) as functions of t. The parameter t interpolates between two points of the band-structure parameters space: $t=0$ corresponds to the particle-hole symmetric case while $t=1$ refers to the parameters that give good agreement with experimental magnetization data (Ref. 20) on $Ba(Fe_{1-x}Co_x)_2As_2$ (see the main text for the actual values).

$$g_{+-}\approx\left[-0.0039+0.0022\left(\frac{\varepsilon_0}{T}\right)^2+0.00008\left(\frac{\varepsilon_0}{T}\right)^4\right]\left(\frac{\delta m}{m}\right)^4 \tag{48}$$

while g_{++} remains close to 2. Since $\varepsilon_0\gg T$, we conclude that the s^{+-} state moves again to the regime of mutual exclusion from antiferromagnetism.

In order for the s^{+-} state to be able to coexist with AFM, we need to consider both a finite chemical potential and a finite ellipticity. Then, depending on the particular values of the band masses, of the energy offsets, and of the chemical potential, g_{+-} will be either positive or negative while g_{++} remains positive.

To illustrate this, we perform a numerical calculation of the coefficients g through a particular path connecting two important points of the parameters space. They are the point with particle-hole symmetry, where $\varepsilon_0\equiv\varepsilon_{1,0}=\varepsilon_{2,0}$, $m_x=m_y=m$, and $\mu=0$, and the point corresponding to the values that consistently describe the magnetic properties of $Ba(Fe_{1-x}Co_x)_2As_2$: $\varepsilon_0=0.110$ eV, $\varepsilon_{1,0}=\varepsilon_0-\mu_0$, $\varepsilon_{2,0}=\varepsilon_0+\mu_0$, $\mu_0=0.015$ eV, $m=1.32m_{\mathrm{electron}}$, $m_x=2m$, $m_y=0.3m$, and $\mu=\mu_c\equiv 0.039$ eV. As we showed in a previous work,[20] these parameters give a satisfactory agreement between our model and the doping and T_N dependence of the experimental values of the relative zero-temperature staggered magnetization in the absence of SC, $M(x,T=0)/M(x=0,T=0)$. The chemical potential μ_c corresponds to a variation in the electronic occupation number by $\Delta n\approx 0.06$ with respect to μ_0. Since each added Co atom replaces one Fe atom, we associate this increase of Δn to the Co doping concentration $x=0.06$.

In particular, the path chosen to connect these two points is parametrized by a real number $t\in[0,1]$, such that $m_x=(1+t^2)m$, $m_y=(1-0.7t)m$, and $\mu=(\mu_c+\mu_0)t^2$. The variation in the electron band ellipticity and in the chemical potential as function of t are shown in Fig. 5, and the corresponding values of g_{+-} and g_{++} are presented in Fig. 6. Clearly, when both ellipticity and μ are finite, g_{+-} can be either positive or

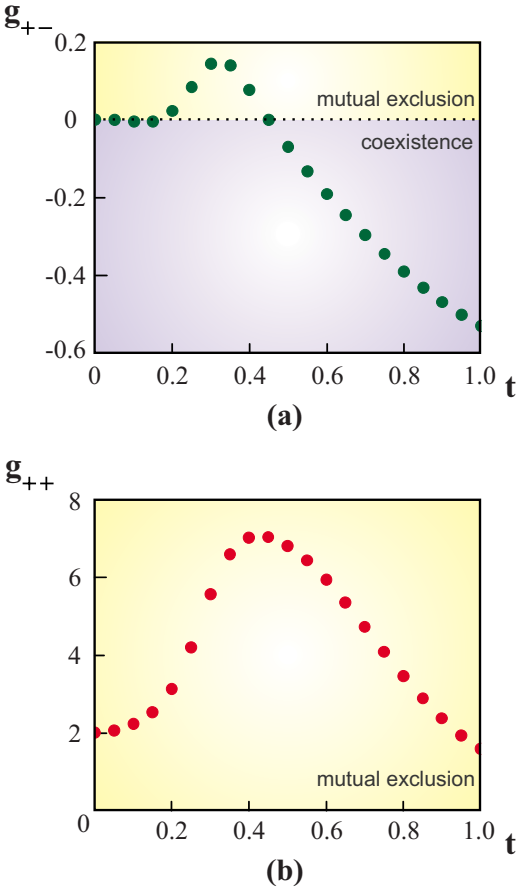

FIG. 6. (Color online) Coupling coefficient g for both (a) the s^{+-} state and (b) the s^{++} state as function of the parameter t, which interpolates between distinct band-structure parameters, changing simultaneously the electron band ellipticity and the chemical potential (see Fig. 5 for the definition of t).

negative, but g_{++} remains positive. Notice that, for the parameters corresponding to $Ba(Fe_{1-x}Co_x)_2As_2$ ($t=1$), the s^{+-} state coexists with magnetism, while the s^{++} state is incompatible with AFM. In particular, for $t=1$, we have

$$g_{+-} \approx -0.52,$$

$$g_{++} \approx 2.0. \tag{49}$$

Our analytical results and numerical calculations indicate that g_{++} is generally positive, in special for the range of parameters associated to the pnictide compounds. In order to investigate this point further, we analyzed which parameters are able to bring g_{++} to smaller values. Particularly, we noticed that by increasing the mass anisotropy of the electron band, while keeping the chemical potential fixed, g_{++} can be reduced. In Fig. 7, we show the effects of an extremely large mass anisotropy on the value of g_{++}. All the other band-structure parameters have the values used before for $t=1$. Clearly, even after pushing the electron band ellipticity to unphysical limits—at least in what concerns the iron arsenides—we still obtain that the s^{++} state cannot coexist with magnetism.

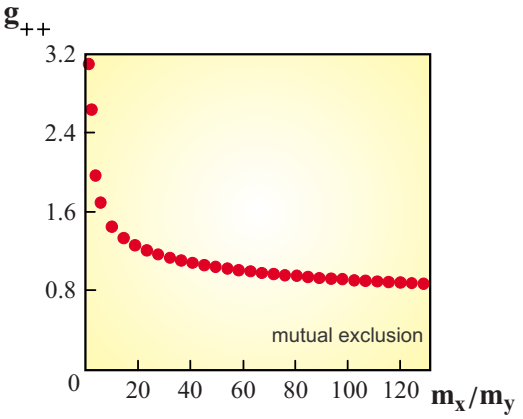

FIG. 7. (Color online) Coupling coefficient g for the s^{++} state as function of the electron band anisotropy m_x/m_y. The values of the other band-structure parameters are described in the text.

These results were briefly discussed in our previous work[20] and, in some detail, by Vavilov *et al.*[41] Considering that $\varepsilon_{1,0}, \varepsilon_{2,0}$ are the dominant energy scales of the problem, the authors of Ref. 41 write the band structure, Eq. (13), in the form $\xi_{2,\mathbf{k}+\mathbf{Q}} = -\xi_{1,\mathbf{k}} - 2\delta_\varphi$, where φ is the angle along the electron pocket and $\delta_\varphi = \delta_0 + \delta_2 \cos 2\varphi$ with δ_0 proportional to the chemical potential and band masses difference and δ_2 to the ellipticity. In this limit, one can approximate $|\Delta_1| \approx |\Delta_2|$ and expand in powers of δ_0 and δ_2. They obtain that g_{+-} becomes negative for a significant range of values where both δ_0 and δ_2 are simultaneously finite. Furthermore, they also find that g_{++} is always positive, in complete agreement with our previous and present results.

Although the Ginzburg-Landau expansion is extremely useful to investigate if SC and AFM are able to coexist, it is formally not valid far from the point where the two phase lines meet. In order to obtain a complete (x,T) phase diagram, including the back bending of the Néel transition line predicted phenomenologically in Sec. II, we self-consistently solve the gap equations [Eq. (20)] at a fixed occupation number. Using the parameters discussed above for $Ba(Fe_{1-x}Co_x)_2As_2$, we obtain the phase diagrams presented in Fig. 1. A zoom of the phase diagram associated to the s^{+-} SC state is presented in Fig. 8, evidencing the reentrance of the AFM transition line. The magnitudes of the electronic interactions were chosen to yield[20] $T_N=140$ K at $x=0$ and $T_c=25$ K at $x=0.06$, and are given by $|V|=0.46$ eV and $I=0.95$ eV. The level of Co doping x is associated to the variation in the electronic occupation number, which depends on the chemical potential. Specifically, we consider that each added Co corresponds to one electron added in the system.

We emphasize that all band-structure parameters were determined in our previous work[20] by fitting the T_N and x dependence of the experimental zero-temperature magnetization, $M(x,T=0)/M(x=0,T=0)$, in the absence of SC. Therefore, in the phase diagram presented in Fig. 1, all the available free parameters are fixed by the shape of the transition lines $T_{N,0}(x)$ and $T_{c,0}(x)$ of the independent uncoupled phases. The actual transition lines $T_N(x)$ and $T_c(x)$ of the system with coupled AFM-SC phases are the solution of the

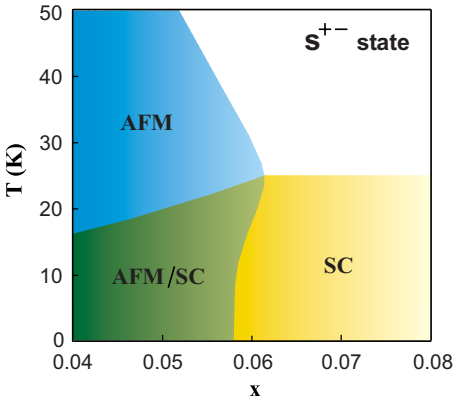

FIG. 8. (Color online) Zoom of the phase diagram of $Ba(Fe_{1-x}Co_x)_2As_2$ considering a superconducting s^{+-} state (see Fig. 1). Note the reentrance of the nonmagnetically ordered phase at low temperatures.

self-consistent gap equations with no extra free parameters involved.

Clearly, the only difference between the phase diagrams for an s^{++} and an s^{+-} SC state is on the coexistence/mutual exclusion regions. In Fig. 9, we compare the temperature dependence of the AFM and SC gaps for a fixed doping in both cases. For $T<T_c$, while in the s^{+-} case the magnetization is strongly suppressed but still survives, in the s^{++} case it completely vanishes once the SC gap opens. Note that, for the s^{+-} case, the $T=0$ values for M and Δ_α are smaller than their values in the respective pure states. In Fig. 10, we present the temperature dependence of the magnetization for several doping values in the case of AFM competing with s^{+-} SC, demonstrating its stronger suppression as the tetracritical point is approached.

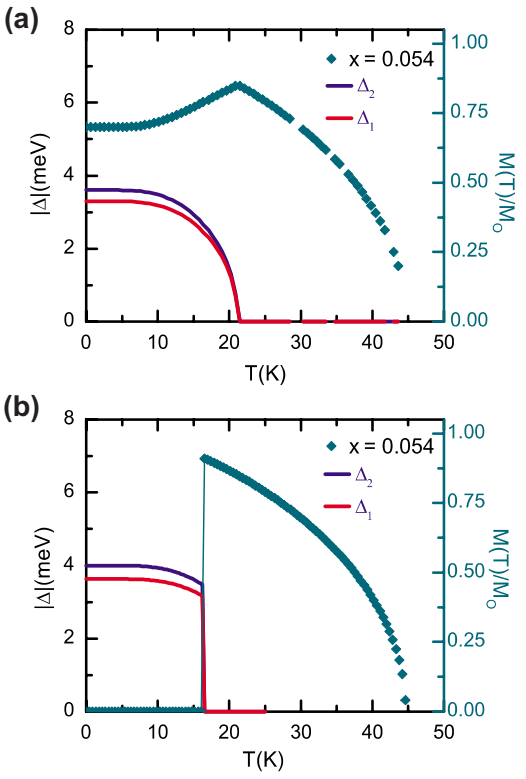

FIG. 9. (Color online) Absolute values of the superconducting order parameters Δ_1 and Δ_2 (in meV), as well as of the magnetic order parameter M [in units of its value M_0 at $(x=0,\ T=0)$] as function of temperature T (in K) for the fixed doping level $x=0.054$ [see the (x,T) phase diagrams of Fig. 1]. Panel (a) shows the result for an s^{+-} state whereas panel (b) presents the result corresponding to an s^{++} state.

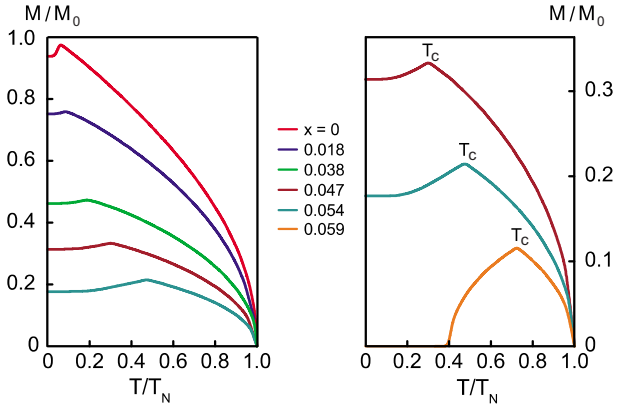

FIG. 10. (Color online) Magnetic order parameter M [in units of its value M_0 at $(x=0,\ T=0)$] as function of temperature T (in units of the AFM transition temperature T_N) for different doping levels. Due to the competition and coexistence with the s^{+-} SC state, M decreases below T_c. Note the reentrant behavior for $x=0.059$. The right panel is a zoom of some of the curves from the left panel.

Numerical calculations of the phase diagram associated to the simplified band structure $\xi_{2,\mathbf{k}+\mathbf{Q}}=-\xi_{1,\mathbf{k}}-2\delta_\varphi$ discussed above were recently presented by Vorontsov *et al.*[42] Our results from Fig. 1 are in general agreement with their findings. Exploring other regions of the parameters space, they also found systems where the s^{+-} coexistence region does not persist all the way to $T=0$ as well as a small region at very low temperatures where s^{++} could, in principle, coexist with AFM.

A rather small region with coexistence between isotropic s-wave SC and itinerant AFM was also found by Kato and Machida[34] in the context of heavy-fermion compounds (see Sec. V for a brief discussion about these materials). Considering a single band without particle-hole symmetry, they performed numerical calculations to determine the phase diagram for different pairing states. In particular, coexistence between isotropic s-wave SC and AFM was only found far from the multicritical point $T_N \simeq T_c$ and in a very narrow regime, analogous to what was reported by Vorontsov *et al.*[42] in the context of the iron arsenides. Note that these results are not in contradiction to our conclusions, since our Ginzburg-Landau expansion and, consequently, the definition of the coupling parameter g_{++}—is only valid for $T_N \simeq T_c$. Far from the multicritical point and from particle-hole symmetry, the details of the bands dispersions are very important and it is, in principle, possible to find coexistence even if $g_{++}>0$ at $T_N \simeq T_c$.

So far, we have only compared the s^{+-} and s^{++} SC states in our calculations. However, electronic theories for the superconductivity in the iron arsenides have also proposed other symmetries for the Cooper-pair wave function where

nodes are present.[50,75,76] One example is the d-wave state, where Δ_1 and/or Δ_2 have nodes along their respective Fermi pockets. The generalization of our formalism to these other symmetry states is straightforward. One has only to introduce the corresponding angular factors $\eta(\varphi)$ for the gaps and for the pairing interaction V, and then average over the Fermi pockets.

In the case of particle-hole symmetry, where the free energy is given by Eq. (46), we obtain, for a d-wave state, $g=(\sqrt{\frac{8}{3}}-1)u\approx 0.6u$. Unlike the s^{+-} state, the d-wave state is not on the borderline between coexistence and mutual exclusion from AFM. However, it is neither deep in the mutual exclusion regime, as the s^{++} state is. Even though the s^{+-} state is the most compatible with itinerant magnetism, we cannot exclude that the d-wave state is also able to coexist with AFM for certain parameters.

C. Incommensurability and the sign of the coupling coefficient

Our model assumes that the magnetism is commensurate. Experimentally, this is still an unsettled issue for $Ba(Fe_{1-x}Co_x)_2As_2$. While neutron-diffraction measurements did not detect any incommensurability inside their resolution window,[17,18,20] some works employing NMR (Ref. 13) and Mössbauer spectroscopy[77] suggest that the magnetism could be weakly incommensurate in these systems.

Theoretically, the weak-coupling model for the excitonic itinerant magnetism naturally predicts the onset of an incommensurate AFM state for small enough temperatures,[78] as recently pointed out by Vorontsov *et al.*[38] To see how this comes out from the model we used here, consider the specific case of detuned bands having the same shape, $\xi_{2,\mathbf{k}+\mathbf{Q}}=-\xi_{1,\mathbf{k}}-2\mu$. Instead of expressing the Ginzburg-Landau coefficients as momentum sums, Eqs. (35), (37), and (39), we can equivalently express them as Matsubara sums. Using the diagrammatic form of the coefficients (see Fig. 4 and Appendix), this is a straightforward calculation and yields

$$u_m = 4\pi\rho T \sum_{\omega_n>0} \frac{\omega_n(\omega_n^2-3\mu^2)}{(\omega_n^2+\mu^2)^3},$$

$$u_{s,\alpha} = 2\pi\rho T \sum_{\omega_n>0} \frac{1}{\omega_n^3},$$

$$\gamma_{\alpha\alpha} = 4\pi\rho T \sum_{\omega_n>0} \frac{\omega_n}{(\omega_n^2+\mu^2)^2},$$

$$\gamma_{\alpha\bar{\alpha}} = 2\pi\rho T \sum_{\omega_n>0} \frac{1}{\omega_n(\omega_n^2+\mu^2)}. \tag{50}$$

Similar expressions were obtained in Ref. 41. Using Eq. (50), it becomes clear now that $u_m<0$ for $T_m^*\lesssim 0.5\mu$, indicating that the transition from the paramagnetic to the commensurate AFM phase is first order. However, as discussed elsewhere,[38] when this condition is met an incommensurate AFM phase has a lower energy than the commensurate state. For the parameters we used to obtain the phase diagrams of $Ba(Fe_{1-x}Co_x)_2As_2$ (Fig. 1), where the Fermi pockets have actually different shapes, the AFM phase line meets the SC phase line before this incommensurate instability takes place. Even if they met after this instability point, it was shown by Vorontsov *et al.*[38,42] that the s^{+-} state remains able to coexist with an incommensurate antiferromagnetic state.

Not only does u_m become negative for low temperatures but also the net coupling coefficient $\gamma\equiv\gamma_{11}+\gamma_{22}\pm 2\gamma_{12}$. Using Eq. (50) for detuned circular bands, we obtain for the s^{+-} case,

$$\gamma_{+-} = 4\pi\rho(\varepsilon_F)T \sum_{\omega_n>0} \frac{\omega_n^2-\mu^2}{\omega_n(\omega_n^2+\mu^2)^2}. \tag{51}$$

Thus, $\gamma_{+-}<0$ for $T^*\lesssim 0.3\mu$. Although the sign of γ_{+-} does not affect the criterion for phase coexistence, $\gamma^2<u_m u_s$, it significantly changes the forms of the AFM and SC transition lines inside the coexistence region. In particular, a negative γ implies that neither T_c nor M are suppressed in the AFM-SC coexistence regime, see, for instance, Eq. (6).

A similar result for the AFM-SC coupling coefficient γ was obtained by Zhang *et al.*[79] in the context of the cuprates. In a weak-coupling calculation at $T=0$ but finite disorder (otherwise the Matsubara sums would diverge), they obtain a negative coupling coefficient between a single-band d-wave SC order parameter and an itinerant AFM order parameter. Technically, the problem of the competition between AFM and a single-band d-wave SC is equivalent to our two-band problem with the s^{+-} SC state. Notice, however, that the coefficient γ_{+-} only becomes negative at $T^*<T_m^*$, i.e., the incommensurate AFM transition would happen before the coupling coefficient changes sign. Thus, γ_{+-} has no meaning in this regime and one would have to go back and calculate the coupling coefficient between an incommensurate AFM order parameter and the SC order parameter. However, the numerical calculations performed by Vorontsov *et al.*[38,42] indicate that this coupling coefficient must be positive. Thus, in our approach, the most stable AFM state and superconductivity are always competing.

Notice that this theoretical discussion about the incommensurability of the AFM state does not take into account the coupling to the lattice degrees of freedom. As argued by many authors, an emergent nematic degree of freedom is present in the iron arsenides due to its frustrated magnetic structure.[80–82] The energy of the system is minimized by the onset of a nematic transition at $T_{\mathrm{nem}}\geq T_N$. Due to the bilinear coupling between the nematic order parameter and the shear distortion, the nematic transition is simultaneous to a structural transition from the tetragonal to the orthorhombic phase. Key to this process is the commensurability of the magnetic fluctuations that give rise to this emergent nematic degree of freedom.[82] Thus, the inclusion of this extra degree of freedom could change the outcome of an incommensurate AFM state at low temperatures.

D. Intraband pairing and Coulomb interaction

In writing our weak-coupling expression for the SC interaction term, Eq. (19), we considered only an interband pairing interaction $V\equiv V_{12}=V_{21}$. If one includes additional intra-

band pairing interactions V_{11} and V_{22}, the only change in the free energy density, Eq. (23), is that the quadratic term $-\frac{1}{V}(\Delta_1^*\Delta_2+\Delta_2^*\Delta_1)$ is replaced by $-\Sigma_{\alpha\beta}(V^{-1})_{\alpha\beta}\Delta_\alpha^*\Delta_\beta$. This will of course change the gap equations, specially the value of T_c, and may also affect the ratio Δ_1/Δ_2. Yet, the inclusion of an intraband pairing interaction will only change the quadratic Ginzburg-Landau coefficients $a_{s,\alpha}$, leaving the values of the quartic coefficients u_s, u_m, and γ unchanged. Since our results regarding the coexistence or mutual exclusion between the SC and AFM states rely solely on the quartic coefficients, they will remain unchanged.

Here, we assume that the interband pairing interaction $V \equiv V_{12}$ is originated from the coupling between electrons and collective modes of the system, such as phonons ($V<0$) or paramagnons ($V>0$), for example. With this in mind, we can investigate the effects of the electronic Coulomb repulsion by adding a renormalized Coulomb interaction $U>0$. First, consider the case of an uniform Coulomb repulsion with equal intraband and interband terms U. Formally, there is now a single interband interaction given by $V+U$, which is enhanced (reduced) in the case of $s^{+-}(s^{++})$ pairing. Yet, due to the different origins of V and U, we here opt to write the total interband interaction in the form $V+U$.

For the pure s^{+-} state, it was previously shown that a uniform renormalized Coulomb interaction U is unable to completely destroy the SC state, i.e., $T_c(U)$ never goes to zero, no matter the magnitude of the Coulomb interaction.[52] In order to demonstrate this, one writes the linearized gap equations in matrix form as $\Delta_\alpha=\Lambda_{\alpha\beta}\Delta_\beta$ and analyzes the eigenvalues of

$$\Lambda = \begin{pmatrix} -U\rho_1 & -(V+U)\rho_2 \\ -(V+U)\rho_1 & -U\rho_2 \end{pmatrix}. \tag{52}$$

The largest eigenvalue λ determines the transition temperature through $\lambda^{-1}=\ln(W/\alpha T_c)$. For small U, it follows that $\lambda=|V|\sqrt{\rho_1\rho_2}-\frac{1}{2}(\sqrt{\rho_1}\pm\sqrt{\rho_2})^2U$, where $+1$ refers to s^{++} pairing and -1 to s^{+-} pairing, respectively. The suppression of the pairing interaction is significantly weaker for the s^{+-} state, in particular, for similar densities of states ρ_1 and ρ_2. For s^{++}-pairing λ, and thus T_c, vanishes as $U\to|V|/2$, while in case of s^{+-} pairing the net pairing interaction stays finite even for infinite U, where it holds $\lambda(U\to\infty)=2|V|\rho_1\rho_2/(\rho_1+\rho_2)$. These results are summarized in Fig. 11.

We next investigate the effects of a uniform Coulomb repulsion in the case where s^{+-} SC coexists with AFM. We now have

$$\Lambda = \begin{pmatrix} -(V+U)r_0 - Ur_2 & -(V+U)r_1 - Ur_0 \\ -(V+U)r_2 - Ur_0 & -(V+U)r_0 - Ur_1 \end{pmatrix}, \tag{53}$$

where

$$r_\alpha = \frac{1}{N}\sum_{\mathbf{k},a} \frac{(E_{a,\mathbf{k}}^2-\xi_{\alpha,\mathbf{k}}^2)\tanh(\beta E_{a,\mathbf{k}}/2)}{2E_{a,\mathbf{k}}(E_{a,\mathbf{k}}^2-E_{\bar{a},\mathbf{k}}^2)},$$

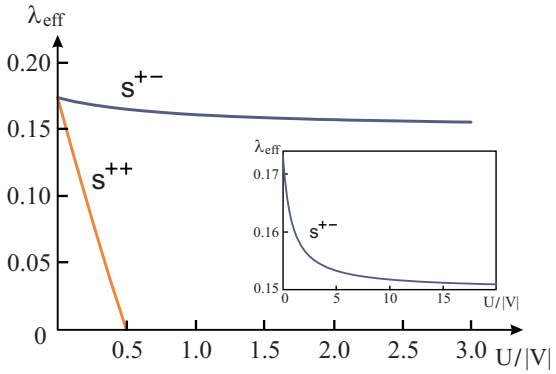

FIG. 11. (Color online) Effective SC coupling constant $\lambda_{\text{eff}}=1/\ln(W/\alpha T_c)$ as function of the ratio between the Coulomb repulsion and the pairing interaction $U/|V|$ for both a pure s^{++} state and a pure s^{+-} state. Here, we considered the values $|V|\rho_1=0.1$ and $|V|\rho_2=0.3$ but the conclusions are similar for arbitrary parameters. The inset is a zoom of the curve associated to the s^{+-} state.

$$r_0 = \frac{1}{N}\sum_{\mathbf{k},a} \frac{M^2\tanh(\beta E_{a,\mathbf{k}}/2)}{2E_{a,\mathbf{k}}(E_{a,\mathbf{k}}^2-E_{\bar{a},\mathbf{k}}^2)} \tag{54}$$

and the excitation energies are given by Eq. (22) with $\Delta_1=\Delta_2=0$. The superconducting transition temperature is again determined by the largest eigenvalue of Λ, which is given by

$$\lambda = -(r_1+r_2+2r_0)U - 2r_0V + [(r_1+r_2+2r_0)^2U^2 + 4r_1r_2V^2 + 4UV(2r_1r_2+r_0r_1+r_0r_2)]^{1/2}. \tag{55}$$

For $U=0$, we find $\lambda=2(\sqrt{r_1r_2}-r_0)V$. Let us assume that, in the absence of the Coulomb interaction, the system undergoes a SC transition at T_c. Imposing the vanishing of the largest eigenvalue, we obtain that $\lambda(U_c)=0$ for $U_c=-V/2$, independent of the value of the magnetic order parameter M or of band-structure details. However, for the s^{+-} case, $V>0$, implying $U_c<0$. Therefore, the s^{+-} SC state inside the antiferromagnetic phase is robust against a uniform Coulomb interaction, similarly to what happens for the nonmagnetic s^{+-} state.

We can also consider the case where the Coulomb interaction is not uniform, such that its value for intraband repulsion U is greater than its value for interband repulsion $U'<U$. Now we need to determine the largest eigenvalue λ of

$$\Lambda = \begin{pmatrix} -(V+U')r_0 - Ur_2 & -(V+U')r_1 - Ur_0 \\ -(V+U')r_2 - Ur_0 & -(V+U')r_0 - Ur_1 \end{pmatrix}. \tag{56}$$

λ now vanishes for $U=|V|\pm U'$, where the plus (minus) sign is to be used for the case of an s^{+-} (s^{++}) state. In this case, both states can be destroyed by a sufficiently large repulsion, yet the s^{++} state is destroyed easier than the s^{+-} state. Note also that the condition $U=|V|\pm U'$ is the same for both situations of a pure SC state and a coexistent SC-AFM state. Thus, in general, magnetism does not seem to significantly influence the ability of the Coulomb repulsion to destroy the SC order. The renormalization of the Coulomb interaction was also investigated using a renormalization-group approach in Ref. 46. Even though the underlying reasoning is somewhat different from our analysis, the con-

clusions of Ref. 46 are consistent with our result. The pair-breaking contribution of the Coulomb interaction is less efficient for the s^{+-} state, if compared to s^{++} superconductivity.

E. Reentrant Néel transition line and quantum fluctuations

According to our phenomenological discussion in Sec. II, the strong suppression of the AFM order parameter in the SC phase is also reflected in the reentrance of the AFM transition line, as shown by the calculated phase diagrams of Fig. 1 and confirmed by neutron-diffraction measurements.[20] The same reentrant behavior is observed in some heavy fermions,[83,84] where AFM-SC coexistence takes place as well. In the cuprates, theoretical models also proposed that a similar reentrance is present in the phase diagram.[85]

Let us investigate in more detail the form of the reentrance line in the iron arsenides. For simplicity, we follow Ref. 41 and consider a small perturbation of the particle-hole symmetric band structure, $\xi_{2,\mathbf{k}+\mathbf{Q}}=-\xi_{1,\mathbf{k}}-2\delta_\varphi$ with $\delta_\varphi=\delta_0+\delta_2\cos 2\varphi$, as we explained in Sec. IV B. Assuming that δ_0 and δ_2 satisfy the conditions for coexistence between AFM and s^{+-} SC, we expand the free energy, Eq. (23), only in powers of M, keeping the SC gap $\Delta=\Delta_1=-\Delta_2$ fixed. This last assumption is justified at low temperatures, where the SC order parameter saturates (see Fig. 9). For $T\ll\delta\ll\Delta$, we obtain for the quadratic magnetic coefficient,

$$a_m(\Delta,T)\approx 4\left(\frac{\Delta-\Delta_c}{\Delta_c}\right)-\left(4\sqrt{2\pi}\frac{\Delta^2\sqrt{T}}{\delta^2\sqrt{\Delta}}\right)e^{-\Delta/T} \qquad (57)$$

with $\delta^2\equiv\langle\delta_\varphi^2\rangle=\delta_0^2+\delta_2^2/2$. Here, Δ_c corresponds to the $T=0$ value of the SC gap where the quantum phase transition from the pure superconducting state to the superconducting state with antiferromagnetic long-range order takes place. Equation (57) implies that, at $T=0$, there is AFM order for $\Delta<\Delta_c$. The negative sign in front of the temperature-dependent term also implies that T_N is finite for $\Delta>\Delta_c$. Therefore, it correctly captures the reentrance of the AFM line.

The presence of the exponential term $e^{-\Delta/T}$ is a consequence of the fact that, inside the SC state, quasiparticle excitations are fully gapped. Due to this exponential dependency, the reentrant T_N line approaches the quantum critical point with an exponentially steep slope, i.e., as an almost vertical line. This is in agreement with our calculated phase diagrams from Fig. 1, as well as with the phase diagrams obtained by Vorontsov *et al.*[42]

These results were derived using a mean-field approach. Close to $T=0$, the presence of quantum fluctuations change this scenario. To illustrate their effects, we consider collective magnetic fluctuations in the vicinity of this quantum critical point. In order to properly describe long-range magnetic order we have to include interlayer coupling and consider an effective three-dimensional quantum rotor model. Due to the fact that quasiparticle excitations are gapped, we consider a rotor model with dynamic critical exponent[86] $z=1$. Within a self-consistent large-N theory, where N refers to the number of components of the rotor, we obtain a renormalization of the coefficient $a_m\to\tilde{a}_m$ due to critical fluctuations,

$$\tilde{a}_m=a_m+u_mT\sum_{\omega_n}\int\frac{d^3q}{(2\pi)^3}\frac{1}{\tilde{a}_m+q^2+\omega_n^2}. \qquad (58)$$

An expansion at low temperatures yields $\tilde{a}_m-a_m=CT^2$ with $C>0$, which dominates over the exponential term $e^{-\Delta/T}$ that follows from the mean-field theory. The presence of power-law corrections in a_m is more general than our self-consistent large-N theory and is expected to occur due to the presence of massless critical fluctuations. Due to the fact that the coefficient C is positive, such quantum fluctuations suppress the magnetic reentrant behavior at very low temperatures. However, as usual in systems in the weak-coupling regime, the critical region where quantum fluctuations are relevant is expected to be very small, and probably hard to be detected experimentally.

V. LOCALIZED VERSUS ITINERANT MAGNETISM

A key conclusion of our calculation is that homogeneous coexistence of superconductivity and magnetism is only allowed in case of unconventional s^{+-}-pairing state while both ordered states exclude each other in case of conventional s^{++} pairing. This conclusion seems to be at odds with the well-known fact that antiferromagnetism and superconductivity do coexist homogeneously in a number of materials where the evidence for conventional electron-phonon pairing is very strong, such as the borocarbides[87] $R\mathrm{Ni}_2\mathrm{B}_2\mathrm{C}$ and the ternary superconductors[88] $R\mathrm{Mo}_6\mathrm{S}_8$ and $R\mathrm{Rh}_4\mathrm{B}_4$, with R denoting a rare earth. The crucial difference between these rare-earth based systems and the iron pnictide superconductors is that the magnetism in the former is due to localized rare-earth spins while in the latter the same electrons that superconduct are responsible for the entire ordered moment. Thus, for our argumentation in the pnictides to hold, it is essential that the same electrons that form the Cooper-pair condensate are responsible for the ordered moment. This is evident from our Hamiltonian, Eq. (11), where the order parameters Δ and M are expectation values of electronic states of the same bands. This is the reason for the highly symmetric form of the free energy of Eqs. (31) and (32) and why the Ginzburg-Landau coefficients for the quartic magnetic, superconducting, and coupling terms are closely related to each other.

In order to demonstrate explicitly that the phase diagram of competing magnetism and superconductivity is very different in case of localized spins, here we analyze this problem in some detail. We recall that the total Hamiltonian is given by $\mathcal{H}_0+\mathcal{H}_{\mathrm{AFM}}+\mathcal{H}_{\mathrm{SC}}$. We keep the same terms for the kinetic and superconducting parts given by Eqs. (12) and (19), respectively. The pairing interaction V in $\mathcal{H}_{\mathrm{SC}}$ might, for example, be due to the electron-phonon interactions. At this point we are not concerned whether systems like the $R\mathrm{Ni}_2\mathrm{B}_2\mathrm{C}$ are indeed characterized by a corresponding two-band model. Instead, we are primarily interested in comparing localized and itinerant magnetism for a system with oth-

erwise unchanged electronic structure. It will become evident below that our analysis is in fact more general. The crucial new term in the Hamiltonian is $\mathcal{H}_{\rm AFM}$ which is replaced by

$$\mathcal{H}_{\rm AFM} = \frac{J_K}{4}\sum_i \mathbf{S}_i \cdot (c_{is}^\dagger \boldsymbol{\sigma}_{ss'} d_{is'} + \text{H.c.}). \tag{59}$$

Here $\mathbf{S}_i$ refers to a localized spin-S operator and J_K is the exchange coupling between localized spins and conduction electrons. We are interested in the regime where J_K leads to magnetic long-range order via the Ruderman-Kittel-Kasuya-Yoshida (RKKY) mechanism with $J_{\rm RKKY}(\mathbf{r}) \simeq J_K^2 \chi_s(\mathbf{r})$, where $\chi_s(\mathbf{r})$ denotes the electronic spin susceptibility. In the regime of antiferromagnetism with large ordered local moments, it is possible to neglect the Kondo effect as $J_{\rm RKKY}$ is larger than the corresponding Kondo temperature. To proceed, we perform a mean-field analysis of this model. We introduce the expectation values

$$\langle S_i^z \rangle = m_{\rm loc} e^{i\mathbf{Q}\cdot\mathbf{R}_i},$$

$$\langle s_i^z \rangle \equiv \frac{1}{2N}\sum_{\mathbf{p}\sigma} \sigma \langle c_{\mathbf{p}\sigma}^\dagger d_{\mathbf{p}+\mathbf{Q}\sigma}\rangle = -m_{\rm el} e^{i\mathbf{Q}\cdot\mathbf{R}_i} \tag{60}$$

with magnetic ordering vector $\mathbf{Q}$. For definiteness, we consider $J_K > 0$, implying that $\langle S_i^z \rangle$ and $\langle s_i^z \rangle$ have opposite sign. Since we ignore the Kondo effect, our final results are independent on the sign of J_K.

In analogy to the theory of itinerant magnetism we perform a mean-field calculation, giving rise to the total free-energy density $F = F_{\rm s} + F_{0,\rm el} + F_{\rm SC}$ with contributions from localized spins, $F_{\rm s}$, from the SC condensate $F_{\rm SC}$, and from the electronic part, $F_{0,\rm el}$, which also includes the order-parameters coupling. The last two terms are completely analogous to the case of an itinerant AFM state competing with SC, Eq. (23), if we identify the magnetic order parameter as

$$M = \frac{J_K m_{\rm loc}}{4}. \tag{61}$$

Recall that M in our notation is the antiferromagnetic potential that causes a gap for Bragg reflected points of the Fermi surface. In case of itinerant magnetism this gap is due to the electron-electron interaction I and the moment of the itinerant electrons. Now the microscopic origin of M is very different. Yet, the expression for the energy of the conduction electrons is still given by

$$F_{0,\rm el} = -2T\sum_{\mathbf{k},a} \ln\left[2\cosh\left(\frac{E_{a,\mathbf{k}}}{2T}\right)\right] \tag{62}$$

with the same excitation energies $E_{a,\mathbf{k}} = E_{a,\mathbf{k}}(\Delta_1, \Delta_2, M)$ from Eq. (22). The contribution to the energy due to the pairing interaction is unchanged as well and given by

$$F_{\rm SC} = -\sum_{\alpha\beta} V_{\alpha\beta}^{-1} \Delta_\alpha^* \Delta_\beta. \tag{63}$$

Finally, the free-energy density due to the localized spins is

$$F_{\rm s} = -T \ln \sum_{m=-S}^{S} e^{m\beta h} + J_K m_{\rm loc} m_{\rm el}, \tag{64}$$

where $h = J_K m_{\rm el}$ is the Weiss field of a single spin S. Since both magnetizations $m_{\rm loc}$ and $m_{\rm el}$ order simultaneously, we can eliminate $m_{\rm el}$ and express the Landau expansion in terms of M. To this end we use $m_{\rm loc} = -\partial F_{\rm s}/\partial h|_{h=J_K m_{\rm el}}$ and solve for $m_{\rm el} = m_{\rm el}(m_{\rm loc})$. Using M of Eq. (61) instead of $m_{\rm loc}$, we find to leading order

$$m_{\rm el} = \frac{T}{\alpha_S J_K^2}\left(M + \frac{\beta_S}{4\alpha_S^3 J_K^2} M^3\right) \tag{65}$$

with

$$\alpha_S = \frac{S(S+1)}{12},$$

$$\beta_S = \frac{S(S+1)[1+2S(S+1)]}{90}. \tag{66}$$

After inserting this result for $m_{\rm el}$ into the free energy, Eq. (64), we can expand it and thus determine the Ginzburg-Landau expansion simultaneously for the SC and AFM order parameters, Δ_1, Δ_2, and M. We obtain the exact same expressions for the coefficients related to the superconducting order parameter, $a_{s,\alpha\beta}$ and $u_{s,\alpha}$, as well as for the coupling $\gamma_{\alpha\beta}$ between the AFM and SC order parameters. Despite the same formal expression, the physical interpretation of the order-parameter coupling terms $\gamma_{\alpha\beta}$ is somewhat different now. It reflects changes in the conduction-electron-mediated RKKY interaction due to the onset of superconductivity.

The only difference in the values of the Ginzburg-Landau parameters due to the presence of localized spins is for the coefficients of the magnetic order parameter. We find

$$a_m = \frac{4T}{\alpha_S J_K^2} - 2\chi_{ph}(\mathbf{Q}) \tag{67}$$

and

$$u_m = u_m^0 + \frac{\beta_S T_N}{(\alpha_S J_K)^4}, \tag{68}$$

where u_m^0 is the quartic coupling of itinerant spins given by Eq. (35). The additional term in Eq. (68) is solely determined by the Néel temperature, T_N, the size of the spin, S, and the coupling J_K. T_N is determined via $a_m(T_N) = 0$ and given, as expected, by the RKKY coupling,

$$T_N = \frac{1}{2}\alpha_S J_K^2 \chi_{ph}(\mathbf{Q}) \tag{69}$$

with bare spin susceptibility of the conduction electrons at the ordering vector $\mathbf{Q}$. Since Eq. (45) gives $u_m^0 \approx \rho/(2T_N^2)$, it follows that the relative change in the magnetic Ginzburg-Landau coefficient is

$$\frac{u_m - u_m^0}{u_m^0} \approx \frac{2\beta_S}{\alpha_S}(J_K\rho)^2 \ln^3(\alpha_S^{-1} J_K^{-2} \rho^{-2}). \tag{70}$$

The additional logarithmic term $\ln^3(\alpha_S^{-1}J_K^{-2}\rho^{-2})$ occurs only near particle-hole symmetry and is replaced by a constant of order unity away from particle-hole symmetry. The prefactor β_S/α_S grows as S^2 for large S. Thus, it is easily possible that the quartic coefficient of the magnetic order parameter is significantly enhanced in case of localized spins. For example, the relative corrections are around 200% for $S=7/2$ and $J_K\rho \simeq 0.025$. Since the order-parameter coupling and the quartic coefficients of the superconducting term are unchanged, it follows that the condition $\gamma < \sqrt{u_s u_m}$ for coexisting order can now be fulfilled easier than in the case of purely itinerant systems. This offers a natural explanation for the observation of homogeneous coexistence of both phases in systems such as the RNi_2B_2C and addresses the fact that coexistence observed in systems with localized spins is not in contradiction to our conclusions. For completeness, we also analyzed a model with additional magnetic interactions between localized spins that are not captured by the RKKY mechanism, adding to $\mathcal{H}_{\mathrm{AFM}}$ of Eq. (59) the term $\frac{1}{2}\Sigma_{i,j}J_{ij}\mathbf{S}_i\cdot\mathbf{S}_j$. This new term will change the value of T_N but not affect the expression, Eq. (68), for u_m.

Additional consequences for localized spins are that the coefficient $a_{m,0}=(\alpha_S J_K^2)^{-1}$ of the temperature-dependent quadratic coefficient $a_m=a_{m,0}(T-T_N)$ is expected to be larger compared to the corresponding coefficient $a_{s,0}\simeq\rho/T_c$ of the superconducting order parameter if we consider the multicritical point $T_c=T_N$ near particle-hole symmetry since $a_{m,0}/a_{s,0}\simeq\chi_{ph}(\mathbf{Q})/\rho$. With Eq. (6) follows then that it becomes harder to achieve a suppression of the magnetization with $d\mathbf{M}^2/dT>0$ below the superconducting transition. The observed suppression[18,19,63] of M in the coexistence region of $Ba(Fe_{1-x}Co_x)_2As_2$ and $Ba(Fe_{1-x}Rh_x)_2As_2$ is therefore an indication that the same electrons are responsible for both states and that magnetism is itinerant in these materials. On the other hand the condition $a_{s,0}\gamma < a_{m,0}u_m$ for suppression of T_c in the magnetically ordered state can easily be fulfilled. Thus, while SC in systems with localized spins is affected by magnetic long-range order, the opposite does not seem to hold and AFM is rather indifferent to SC.

Finally we comment on the relevance of this calculation for heavy-fermion superconductors, such as $CeRhIn_5$ and UPt_3. In $CeRhIn_5$, the coexistence between magnetism and superconductivity has been investigated in great detail[83] while in UPt_3 there is clear evidence[84] for suppression of magnetism below T_c. The heavy-fermion system are believed to be properly described by the Kondo lattice Hamiltonian[89] with coupling between localized and conduction electrons as in $\mathcal{H}_{\mathrm{AFM}}$ of Eq. (59). However, our analysis of this model, where we completely ignored the Kondo effect and the emergence of a heavy electron state is inadequate for such systems. In fact one expects that a system in the heavy electron state is better described by the theory employed here for the FeAs systems, yet the interactions I and V as well as the quasiparticles masses are heavily renormalized due to Kondo lattice screening. Thus, while a detailed theory for the competition of magnetism and superconductivity in heavy electron states is complex, we do expect a similar competition in the FeAs systems and these heavy-fermion compounds. The very similar behavior of the SC and AFM transition lines in the phase diagrams[20,83,85] of $Ba(Fe_{1-x}Co_x)_2As_2$ and $CeRhIn_5$, as well as the suppression of the magnetization[84] of UPt_3 below T_c, certainly support this view.

VI. SUPPRESSION OF SC IN THE OVERDOPED REGION

So far we have analyzed the competition between AFM and SC with the consequent suppression of the superconducting state in the underdoped region of the phase diagram of the iron arsenides. In the overdoped region there is no magnetically ordered state, yet SC is also suppressed and eventually disappears. The Fermi surface in this part of the phase diagram also changes significantly: for electron (hole) doped samples, it is characterized by increasingly large electron (hole) pockets and decreasingly small hole (electron) pockets,[53] which eventually disappear at a certain doping level. In this section, we investigate how the disappearance of these pockets from the Fermi surface affects the transition temperature of the pure SC state.

We consider, once more, one hole pocket centered at the Brillouin zone and one electron pocket displaced by $\mathbf{Q}$ from the zone center. For definiteness, we use the band dispersions, Eq. (13), with $\varepsilon_0\equiv\varepsilon_{1,0}=\varepsilon_{2,0}$ and vary the chemical potential μ. Here, we consider the effects of electron doping only, such that $\mu>0$; the case of hole doping ($\mu<0$) is analogous and the same conclusions hold. For simplicity, we first consider V to be constant as μ changes and neglect intraband pairing interactions. The linearized gap equations are then given by

$$\Delta_1 = -\frac{V\Delta_2}{2}\int_{-W}^{W} d\xi \rho_2(\xi)\frac{\tanh\left(\frac{\xi}{2T_c}\right)}{\xi},$$

$$\Delta_2 = -\frac{V\Delta_1}{2}\int_{-W}^{W} d\xi \rho_1(\xi)\frac{\tanh\left(\frac{\xi}{2T_c}\right)}{\xi}, \tag{71}$$

where, once again, W denotes an upper energy cutoff associated to the pairing interaction. In a two-dimensional (2D) system, the density of states $\rho_i(\xi)$ is constant if the energy ξ falls inside the bands. Therefore, diagonalization of the linearized gap equations give the following implicit expression for T_c:

$$\frac{1}{\lambda_0^2} = \int_{-(W/2T_c)}^{(\varepsilon_0-\mu/2T_c)} dx \int_{-\min[(W/2T_c),(\varepsilon_0+\mu/2T_c)]}^{(W/2T_c)} dy \frac{\tanh x \tanh y}{4xy}, \tag{72}$$

where we introduced $\lambda_0=V\sqrt{\rho_1\rho_2}$. For simplicity, let us first consider the special case $W=\varepsilon_0$; the main conclusions hold for an arbitrary W.

Although a complete analytical solution for $T_c(\mu)$ is not available from Eq. (72), we can obtain some important limits. For small $\mu \ll \varepsilon_0$, we obtain that T_c decreases linearly with respect to $T_c^{(0)}\equiv T_c(\mu=0)$,

$$T_c = T_c^{(0)}\left(1-\frac{\mu}{4\varepsilon_0}\right). \tag{73}$$

Equivalently, we can show that the effective coupling constant $\lambda_{\text{eff}} \equiv \ln^{-1}\left(\frac{W}{T_c}\frac{2e^{\gamma_E}}{\pi}\right)$ decreases linearly with μ from its $\mu=0$ value λ. At the special point $\mu=\varepsilon_0$, i.e., when the hole pocket shrinks to a single point in the Fermi surface, the effective coupling constant is reduced to about 70% of its initial value, $\lambda_{\text{eff}}=\lambda/\sqrt{2}$, implying

$$T_c = T_c^{(0)} e^{-\sqrt{2}-1/\lambda}. \tag{74}$$

Even though the vanishing of the hole pocket does not cause T_c to vanish, it does signal the onset of a regime where the coupling constant decays very strongly with respect to the chemical potential μ, in contrast to the case of small chemical potential, where the decay λ_{eff} was linear in μ. To illustrate this point, consider the regime of $\varepsilon_0 < \mu < 2\varepsilon_0$ such that $\mu - \varepsilon_0 \gg T_c$. Notice that this condition is not too restrictive, since $T_c < T_c^{(0)} \ll \varepsilon_0$, by construction. Then, it follows that

$$\lambda_{\text{eff}} = \frac{\lambda^2}{2}\ln\left(\frac{\varepsilon_0}{\mu-\varepsilon_0}\right) \tag{75}$$

implying

$$T_c = T_c^{(0)} \exp\left[-\frac{2}{\lambda^2 \ln\left(\frac{\varepsilon_0}{\mu-\varepsilon_0}\right)} + \frac{1}{\lambda}\right] \tag{76}$$

Clearly, the effective coupling constant only vanishes at $\mu = W + \varepsilon_0 = 2\varepsilon_0$, i.e., where the range of energies for which the net attractive interaction is positive does not cross the hole pocket. However, it is already significantly reduced for values of the chemical potential much smaller than that one. In Fig. 12, we present the behavior of T_c for two values of the effective zero-doping coupling constant, $\lambda_0=0.2$ and $\lambda_0=0.3$. Notice that, in both cases, T_c decreases moderately for $\mu < \varepsilon_0$ (i.e., when the hole pocket is small but still present) and then is strongly reduced for $\mu > \varepsilon_0$ (i.e., when the hole pocket disappears from the Fermi surface). The same conclusions also hold for the case of an arbitrary cutoff $W > \varepsilon_0$: the special point of the phase diagram where the hole pocket is reduced to a Fermi point marks the onset of a dramatic reduction of T_c, no matter the initial value of the coupling constant λ_0.

As we mentioned, T_c actually only vanishes at $\mu = W + \varepsilon_0$. However, in this region where it is strongly suppressed, even a uniform Coulomb interaction is able to completely destroy superconductivity. This is to be contrasted to the optimally doped region, where the s^{+-} state is robust against a uniform Coulomb repulsion, as we discussed in the previous section.

To illustrate how the s^{+-} SC state is killed in the region of strong suppression, $\mu - \varepsilon_0 \gg T_c$, consider $W=\varepsilon_0$ and an uniform repulsion $U>0$. For simplicity, we focus only on the limit of $U \gg V$. To leading order, the equation determining the effective SC coupling constant is given by

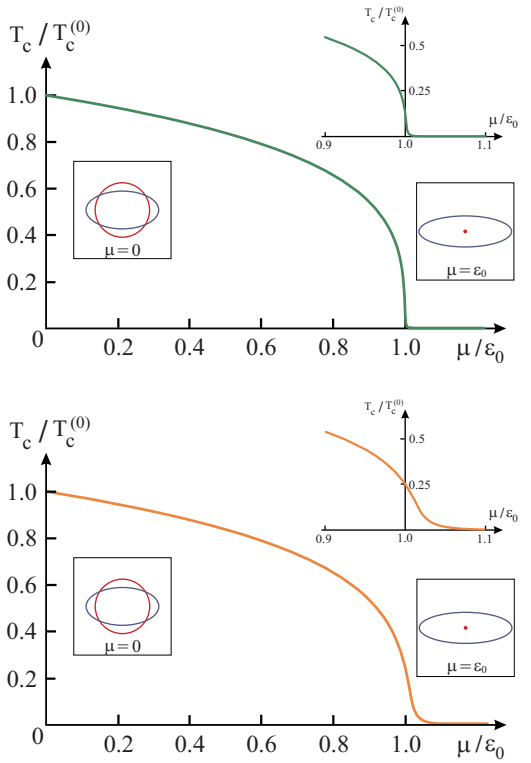

FIG. 12. (Color online) Superconducting transition temperature T_c (in units of its value at zero chemical potential $T_c^{(0)}$) as function of the chemical potential μ (in units of ε_0) for both an initial effective SC coupling (a) $\lambda_0=0.2$ and (b) $\lambda_0=0.3$. The insets show the changes in the Fermi surface with μ, with the red circle (blue ellipse) denoting the hole (electron) pocket. In the upper right corner of each panel we present a zoom of the region around $\mu=\varepsilon_0$ where the electron pocket is reduced to a Fermi point.

$$\frac{2\ln\left(\frac{\varepsilon_0}{\mu-\varepsilon_0}\right)V\rho_1\rho_2}{\lambda_{\text{eff}}\ln\left(\frac{\varepsilon_0}{\mu-\varepsilon_0}\right)\rho_1 + 2\rho_2} = 1. \tag{77}$$

Defining $\lambda_i = V\rho_i$, we obtain

$$\lambda_{\text{eff}} = \frac{2\lambda_2}{\lambda_1}\left[\lambda_1 - \frac{1}{\ln\left(\frac{\varepsilon_0}{\mu-\varepsilon_0}\right)}\right]. \tag{78}$$

Note that λ_{eff} vanishes at $\mu^* = \varepsilon_0(1+e^{-1/\lambda_1})$ but is positive for $\mu < \mu^*$. Thus, a sufficiently large Coulomb interaction U is now able to destroy the s^{+-} SC state, contrary to what happened when the hole pocket was part of the Fermi surface, where $\lambda_{\text{eff}} \to \text{const}$ even as $U \to \infty$.

The previous analysis holds for a 2D system. In the case of a three-dimensional system, the density of states is not constant anymore, but given by $\rho_1(\xi) = c_1\sqrt{\varepsilon_0 - \mu - \xi}$ for the hole band and by $\rho_2(\xi) = c_2\sqrt{\varepsilon_0 + \mu + \xi}$ for the electron band. Here, we neglected the anisotropy of the electron band and denoted unimportant constants by c_i. The main difference from the two-dimensional case is that the densities of states go to zero at the bands edges, leading to a significant stron-

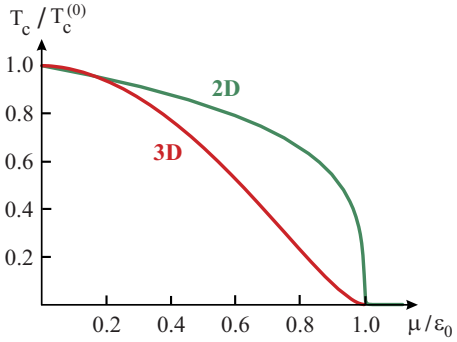

FIG. 13. (Color online) Comparison between the behavior of T_c (in units of its value at zero chemical potential $T_c^{(0)}$) as function of the chemical potential μ (in units of ε_0) for a two-dimensional and a three-dimensional system (green and red curves, respectively). The coupling constants were chosen to give $T_c^{(0)} \approx 0.03W$ in both cases with $W=\varepsilon_0$.

ger reduction in T_c as the chemical potential increases. This is illustrated in Fig. 13, where we compare the solutions of the linearized gap equations [Eqs. (71)] for the cases of a 2D and a 3D system, with coupling constants chosen to yield $T_c(\mu=0) \approx 0.03W$. Therefore, close to the point of the phase diagram where the hole pocket disappears, the space dimensionality matters much more than in the usual Cooper problem.

Our results suggest that the main factor responsible for the complete suppression of the SC state in the overdoped region of the iron arsenides phase diagram is the evolution of the Fermi surface with doping. This is corroborated by ARPES measurements[57–59] on $Ba(Fe_{1-x}Co_x)_2As_2$, which show no superconductivity in the overdoped region after the Fermi surface loses one of its pockets around $x \approx 0.15$. The fact that superconductivity requires the presence of the hole pocket and the observation that the superconducting gap on the hole and electron pockets are very similar, strongly support the view that the pairing interaction in the pnictides is due to interband coupling.

VII. CONCLUDING REMARKS

We showed that the ability of superconductivity and antiferromagnetism to order simultaneously depends sensitively on the nature of the Cooper-pair wave function. In a two-band system with particle-hole symmetry, the itinerant AFM state and the unconventional s^{+-} SC state are exactly in a borderline regime between phase coexistence and phase separation. In contrast, the conventional s^{++} state is deep in the regime of mutual phase exclusion. We further demonstrated that this result holds regardless of additional details of the band structure or the system's dimensionality. It does not change either when one considers the presence of intraband pairing interactions or the effects of Coulomb repulsion. The robustness of this result, valid around the multicritical point $T_N \simeq T_c$, is related to the quasiparticle excitation spectrum of the system, which depends on the peculiar combination $\mathbf{M}^2 + |\Delta|^2 \equiv \vec{\mathbf{N}}^2$ only. This is the root of the SO(5) symmetry of the free-energy expansion, which has been shown to hold not only in the mean-field level, but also in the strong-coupling limit, as a subgroup of an emergent SO(6) symmetry present in the Hamiltonian.[66] Furthermore, the inclusion of fluctuations in our free-energy expansion are known to not change the condition for having the borderline regime,[61,62] $g=0$. All these facts suggest that this simple result is a much more general property of this type of system. We also demonstrated that for our results to hold, it is crucial that the same electrons that form Cooper pairs are responsible for the formation of the ordered moment. For instance, we showed that an AFM state generated by localized moments has a tendency of being indifferent to SC, falling much easier in the regime of phase coexistence.

When applying this result to the pnictides, one has to critically evaluate whether the assumptions that were made are too restrictive. We assumed a certain vicinity to particle-hole symmetry. It is evident that the real materials do not have perfectly nested bands.[53] Yet, there are clearly two sets of pockets whose centers are separated by the ordering vector $\mathbf{Q}$. As we showed, small perturbations in the ellipticity of one pocket or in the chemical potential bring the s^{+-} state to the regime of mutual exclusion. However, simultaneous perturbations in both quantities can bring the system to either regime, as our Fig. 6 illustrates. Most importantly, small deviations from perfect nesting are not sufficient to lead to simultaneous order of magnetism and s^{++} pairing close to the multicritical point. The fact that particular details of the band structure are able to bring the s^{+-} state either to the phase coexistence or to the phase separation regime is, in our view, what makes some of the iron arsenides display second-order AFM-SC transition and others, first-order AFM-SC transition. For $Ba(Fe_{1-x}Co_x)_2As_2$, we were able to independently "fit" the effective band-structure parameters to give the correct doping and T_N dependence of the zero-temperature magnetization in the absence of superconductivity.[20] Having this set of parameters, which did not depend on any SC property, we were able to obtain the complete mean-field x-T phase diagram and to readily calculate the parameter g, verifying that, as evidenced by many experimental probes,[7,8,13–19] $Ba(Fe_{1-x}Co_x)_2As_2$ has homogeneous coexistence between SC and AFM states.

For other compounds that are believed to display phase separation, such as $LaFeAs(O_{1-x}F_x)$ and $(Ba_{1-x}K_x)Fe_2As_2$, we do not have the same systematic diffraction measurements that allow a reliable extraction of effective two-band parameters. Even though tight-binding fits to density-functional theory calculated band structures are available, they usually refer to the parent compounds. The problem to extrapolate them to finite doping is that, in these materials, doping is not on the Fe site nor on the FeAs plane, which makes it much more difficult to make a direct association between electronic occupation number and doping level, as we did for $Ba(Fe_{1-x}Co_x)_2As_2$. Furthermore, in some of the pnictides, the issue of whether they have homogeneous or heterogeneous AFM-SC coexistence is still not completely settled. For example, in $(Ba_{1-x}K_x)Fe_2As_2$, while many experiments find phase separation, Mössbauer spectroscopy identifies microscopic coexistence.[90] In $SmFeAs(O_{1-x}F_x)$, muon-spin rotation[6] finds homogeneous coexistence while a work combining powder x-ray diffraction, Mössbauer spec-

troscopy, and nuclear resonant forward scattering finds phase separation.[91]

In what concerns the pairing state, although many theories for pairing due to electronic interactions predict a nodeless s^{+-} state, other models also suggest that accidental (i.e., not related to symmetry) nodes[49,75,76] or even d-wave nodal states[50] could be present. Furthermore, penetration depth experiments are, in principle, consistent with the existence of accidental nodes.[92] The inclusion of gap nodes in our model, as we discussed, tend to move the SC state from the borderline regime to the mutual exclusion regime, although not as deep as in the s^{++} case. Clearly, A_{1g} sign-changing gap functions with specific configurations of nodes could be as effective as small perturbations of the particle-hole symmetric band structure in making the AFM-SC state go from one regime to the other. Thus, while we cannot discard the presence of unconventional nodal states coexisting with AFM, we can certainly discard the conventional s^{++} state: it is simply incompatible with magnetism.

Regarding the nature of the magnetic state, there is still some debate whether the AFM phase is due to conduction electrons or localized spins. Our analysis shed light on this subject: as our calculations demonstrated, a magnetically ordered phase with localized spins can coexist much easier with superconductivity. This holds even for conventional BCS states, like in the case of the ternary[88] and quaternary[87] rare-earth compounds. Furthermore, the magnetization is not so affected by the SC condensate as in the case of purely itinerant magnetism. Therefore, the experimental observation of reentrance of the paramagnetic phase inside the SC dome[20] seems to rule out the AFM state formed only by localized moments.

As we showed, in the underdoped side of the FeAs phase diagram, both T_N and T_c are suppressed due to the competition between the AFM and SC phases. The Néel transition line is even bent back, approaching the x axis vertically, similar to the case of a first-order transition line. The suppression of T_c is milder; this difference is probably due to the fact that the AFM gap opens only around the corresponding Bragg scattered points,[40] whereas the SC gap opens isotropically around the Fermi surface. In the overdoped side, however, SC is the only thermodynamic ordered phase of the system and yet it is suppressed similarly to the underdoped side. Our calculations using the coupled SC gap equations shows that this suppression is related to the disappearance of one of the pockets from the Fermi surface. As suggested by our Figs. 12 and 13, and by ARPES measurements[57–59] in $Ba(Fe_{1-x}Co_x)_2As_2$, the main cause of suppression of SC in the overdoped side seems to be the doping-induced changes in the Fermi surface rather than possible changes in the magnitude of the pairing interaction. Interestingly, the Fermi surface is also indirectly responsible for the suppression of T_c in the underdoped side since it is the driving force of the AFM instability.[27]

The calculations we presented here did not take into account another important degree of freedom present in the iron arsenides, the orthorhombic distortion. However, in separate works, we showed that the competition between SC and AFM, combined with the coupling between nematic degrees of freedom and structural distortion, are able to consistently explain the observed back bending of the structural transition line[93] inside the SC dome as well as the increase in the shear modulus[82] below T_c.

Finally, we comment that in many models of unconventional pairing in the iron arsenides, the bosons responsible for the formation of Cooper pairs are spin fluctuations.[44–46,49–51] In this case, the pairing interaction V itself would also be sensitive to the presence of magnetic long-range order. Clearly, this would change some details of the coexistence state, particularly the form of the transition lines. Yet, our main conclusions still hold in this case, since the decision about the coexistence between AFM and SC is made when both transition temperatures are close, implying that the order parameters are only infinitesimal.

ACKNOWLEDGMENTS

We thank S. Bud'ko, P. Canfield, P. Chandra, A. Chubukov, A. Goldman, D. Johnston, A. Kaminski, A. Kreyssig, R. McQueeney, D. Pratt, R. Prozorov, S. Sachdev, and M. Vavilov for fruitful discussions. This work was supported by the U.S. DOE, Office of BES, DMSE. Ames Laboratory is operated for the U.S. DOE by Iowa State University under Contract No. DE-AC02–07CH11358.

APPENDIX: DIAGRAMMATIC INTERPRETATION OF THE GINZBURG-LANDAU COEFFICIENTS

Here, we rederive the Ginzburg-Landau expansion in Eq. (23) by explicitly integrating out the fermionic degrees of freedom of a system with competing SC and AFM. This method is useful since it provides a diagrammatic interpretation for the coefficients, as presented in Fig. 4. We first define the Nambu operator

$$\psi_{\mathbf{k}} = (c_{\mathbf{k}\uparrow} \quad c^{\dagger}_{-\mathbf{k}\downarrow} \quad d_{\mathbf{k}+\mathbf{Q}\uparrow} \quad d^{\dagger}_{-\mathbf{k}-\mathbf{Q}\downarrow})^T \tag{A1}$$

and generalize the uniform order parameters Δ_α and M to inhomogeneous functions of space and time $\Delta_{\alpha,(\mathbf{k},\omega_n)}$ and $M_{(\mathbf{k},\omega_n)}$, where $\omega_n=(2n+1)\pi T$ is a fermionic Matsubara frequency. Thus, denoting $k=(\mathbf{k},\omega_n)$, we obtain the Green's function,

$$\hat{\mathcal{G}}^{-1}_{k,k'} = (i\omega_n - \hat{\xi}_{\mathbf{k}})\delta_{k,k'} - \hat{U}_{k-k'}, \tag{A2}$$

where the hat denotes a matrix in Nambu space and

$$\hat{U}_{k-k'} = \hat{\Delta}_{k-k'} + \hat{M}_{k-k'}. \tag{A3}$$

With the help of the Pauli matrices $\boldsymbol{\tau}$, we can write the 4×4 Nambu matrices as

$$\hat{\xi}_{\mathbf{k}} = \begin{pmatrix} \xi_{1,\mathbf{k}}\tau_z & 0 \\ 0 & \xi_{2,\mathbf{k}+\mathbf{Q}}\tau_z \end{pmatrix} \tag{A4}$$

and

$$\hat{\Delta}_q = \begin{pmatrix} -\Delta_{1,q}\tau_x & 0 \\ 0 & -\Delta_{2,q}\tau_x \end{pmatrix} \tag{A5}$$

as well as

$$\hat{M}_q = \begin{pmatrix} 0 & -M_q\tau_0 \\ -M_q\tau_0 & 0 \end{pmatrix}. \tag{A6}$$

Therefore, after introducing the condensation energy of the magnetic and superconducting phases, we obtain the action,

$$S = \int_k \psi_k^\dagger \hat{\mathcal{G}}^{-1}_{k,k'} \psi^\dagger_{k'} + 2\int_x \left[\frac{M^2}{I} - \frac{\Delta_1\Delta_2}{V}\right], \tag{A7}$$

where $\int_k = T\Sigma_n \Sigma_{\mathbf{k}}$ and $\int_x = \frac{1}{v}\int d^d x \int_0^{T^{-1}} d\tau$ with v denoting the volume of the system. The fermions can now be integrated out, yielding an effective action in terms of the collective AFM and SC fields S_{eff}. The partition function of the free fermions is given by

$$Z_0 = \det(-\hat{\mathcal{G}}_0^{-1}), \tag{A8}$$

where we defined the noninteracting Nambu Green's function $\hat{\mathcal{G}}^{1-}_{0,kk'} = (i\omega_n - \hat{\xi}_{\mathbf{k}})\delta_{k,k'}$. The effective action reads

$$S_{\text{eff}} = -\operatorname{Tr}\ln(1 - \hat{\mathcal{G}}_0\hat{U}) + 2\int_x \left(\frac{M}{I} - \frac{\Delta_1\Delta_2}{V}\right). \tag{A9}$$

Here, the trace refers to the sum over momentum, frequency, and Nambu indices. Notice that, for uniform AFM and SC gaps, the total free-energy density (free-fermions contribution included) is given by

$$f = -\int_k \ln\det(\hat{\mathcal{G}}^{-1}_{k,k'}) + \frac{2M^2}{I} - \frac{2\Delta_1\Delta_2}{V}. \tag{A10}$$

Since $\det(\hat{\mathcal{G}}^{-1}_{k,k'}) = \Sigma_{\mathbf{k},a}(\omega_n^2 + E^2_{a,\mathbf{k}})$, we can evaluate the Matsubara sum to obtain

$$f = -2T\sum_{\mathbf{k},a} \ln\left[2\cosh\left(\frac{E_{a,\mathbf{k}}}{2T}\right)\right] + \frac{2M^2}{I} - \frac{2\Delta_1\Delta_2}{V} \tag{A11}$$

with excitation energies $E_{a,\mathbf{k}}$ given by the positive roots of Eq. (22). Minimization of the free energy, Eq. (A11), with respect to Δ_α and M leads then to the gap equations [Eq. (20)].

Going back to the effective action, Eq. (A9), we can now perform a Ginzburg-Landau expansion in the AFM and SC order parameters. Expansion of the logarithm yields, for the free energy relative to the paramagnetic, normal phase

$$\delta F = \frac{1}{2}\operatorname{Tr}(\hat{\mathcal{G}}_0\hat{U})^2 + \frac{1}{4}\operatorname{Tr}(\hat{\mathcal{G}}_0\hat{U})^4 + 2\int_x \left(\frac{M^2}{I} - \frac{\Delta_1\Delta_2}{V}\right). \tag{A12}$$

Considering static and homogeneous AFM and SC gaps and performing the traces in the Nambu space, we obtain the free-energy density expansion of Eq. (23) with Ginzburg-Landau coefficients,

$$a_m = \frac{4}{I} + 4\int_k G_{1,k}G_{2,k},$$

$$a_{s,\alpha\beta} = -\frac{2}{V}(1-\delta_{\alpha\beta}) - 2\delta_{\alpha\beta}\int_k G_{\alpha,k}G_{\alpha,-k},$$

$$u_m = 4\int_k G^2_{1,k}G^2_{2,k},$$

$$u_{s,\alpha} = 2\int_k G^2_{\alpha,k}G^2_{\alpha,-k},$$

$$\gamma_{\alpha\alpha} = -4\int_k G_{\alpha,k}G_{\alpha,-k}G_{1,k}G_{2,k},$$

$$\gamma_{\alpha\bar{\alpha}} = 2\int_k G_{\alpha,k}G_{\alpha,-k}G_{\bar{\alpha},k}G_{\bar{\alpha},-k}. \tag{A13}$$

In the previous expressions, we introduced the noninteracting single-particle Green's function $G_{1,k} = (i\omega_n - \xi_{1,\mathbf{k}})^{-1}$ and $G_{2,k} = (i\omega_n - \xi_{2,\mathbf{k}+\mathbf{Q}})^{-1}$. Thus, the coefficients depend only on the band structure and on the magnitude of the electronic interactions. The Feynman diagrams associated to the quartic coefficients of Eq. (A13) are presented in Fig. 4. Evaluation of the Matsubara sums then leads to Eqs. (35), (37), and (39) for the Ginzburg-Landau coefficients.

*rafaelmf@ameslab.gov

[1] Y. Kamihara, T. Watanabe, M. Hirano, and H. Hosono, J. Am. Chem. Soc. **130**, 3296 (2008).

[2] X. H. Chen, T. Wu, G. Wu, R. H. Liu, H. Chen, and D. F. Fang, Nature (London) **453**, 761 (2008).

[3] G. F. Chen, Z. Li, D. Wu, G. Li, W. Z. Hu, J. Dong, P. Zheng, J. L. Luo, and N. L. Wang, Phys. Rev. Lett. **100**, 247002 (2008).

[4] M. Rotter, M. Tegel, and D. Johrendt, Phys. Rev. Lett. **101**, 107006 (2008).

[5] H. Luetkens, H.-H. Klauss, M. Kraken, F. J. Litterst, T. Dellmann, R. Klingeler, C. Hess, R. Khasanov, A. Amato, C. Baines, M. Kosmala, O. J. Schumann, M. Braden, J. Hamann-Borrero, N. Leps, A. Kondrat, G. Behr, J. Werner, and B. Büchner, Nature Mater. **8**, 305 (2009).

[6] A. J. Drew, Ch. Niedermayer, P. J. Baker, F. L. Pratt, S. J. Blundell, T. Lancaster, R. H. Liu, G. Wu, X. H. Chen, I. Watanabe, V. K. Malik, A. Dubroka, M. Rössle, K. W. Kim, C. Baines, and C. Bernhard, Nature Mater. **8**, 310 (2009).

[7] N. Ni, M. E. Tillman, J.-Q. Yan, A. Kracher, S. T. Hannahs, S. L. Bud'ko, and P. C. Canfield, Phys. Rev. B **78**, 214515 (2008).

[8] J.-H. Chu, J. G. Analytis, C. Kucharczyk, and I. R. Fisher, Phys. Rev. B **79**, 014506 (2009).

[9] C. R. Rotundu, D. T. Keane, B. Freelon, S. D. Wilson, A. Kim, P. N. Valdivia, E. Bourret-Courchesne, and R. J. Birgeneau, Phys. Rev. B **80**, 144517 (2009).

[10] T. Goko, A. A. Aczel, E. Baggio-Saitovitch, S. L. Bud'ko, P. C.

Canfield, J. P. Carlo, G. F. Chen, P. Dai, A. C. Hamann, W. Z. Hu, H. Kageyama, G. M. Luke, J. L. Luo, B. Nachumi, N. Ni, D. Reznik, D. R. Sanchez-Candela, A. T. Savici, K. J. Sikes, N. L. Wang, C. R. Wiebe, T. J. Williams, T. Yamamoto, W. Yu, and Y. J. Uemura, Phys. Rev. B **80**, 024508 (2009).

[11] H. Fukazawa, T. Yamazaki, K. Kondo, Y. Kohori, N. Takeshita, P. M. Shirage, K. Kihou, K. Miyazawa, H. Kito, H. Eisaki, and A. Iyo, J. Phys. Soc. Jpn. **78**, 033704 (2009).

[12] J. T. Park, D. S. Inosov, C. Niedermayer, G. L. Sun, D. Haug, N. B. Christensen, R. Dinnebier, A. V. Boris, A. J. Drew, L. Schulz, T. Shapoval, U. Wolff, V. Neu, X. P. Yang, C. T. Lin, B. Keimer, and V. Hinkov, Phys. Rev. Lett. **102**, 117006 (2009).

[13] Y. Laplace, J. Bobroff, F. Rullier-Albenque, D. Colson, and A. Forget, Phys. Rev. B **80**, 140501(R) (2009).

[14] M.-H. Julien, H. Mayaffre, M. Horvatic, C. Berthier, X. D. Zhang, W. Wu, G. F. Chen, N. L. Wang, and J. L. Luo, EPL **87**, 37001 (2009).

[15] C. Bernhard, A. J. Drew, L. Schulz, V. K. Malik, M. Rossle, C. Niedermayer, T. Wolf, G. D. Varma, G. Mu, H. H. Wen, H. Liu, G. Wu, and X. H. Chen, New J. Phys. **11**, 055050 (2009).

[16] F. Ning, K. Ahilan, T. Imai, A. S. Sefat, R. Jin, M. A. McGuire, B. C. Sales, and D. Mandrus, J. Phys. Soc. Jpn. **78**, 013711 (2009).

[17] C. Lester, J.-H. Chu, J. G. Analytis, S. C. Capelli, A. S. Erickson, C. L. Condron, M. F. Toney, I. R. Fisher, and S. M. Hayden, Phys. Rev. B **79**, 144523 (2009).

[18] D. K. Pratt, W. Tian, A. Kreyssig, J. L. Zarestky, S. Nandi, N. Ni, S. L. Bud'ko, P. C. Canfield, A. I. Goldman, and R. J. McQueeney, Phys. Rev. Lett. **103**, 087001 (2009).

[19] A. D. Christianson, M. D. Lumsden, S. E. Nagler, G. J. MacDougall, M. A. McGuire, A. S. Sefat, R. Jin, B. C. Sales, and D. Mandrus, Phys. Rev. Lett. **103**, 087002 (2009).

[20] R. M. Fernandes, D. K. Pratt, W. Tian, J. L. Zarestky, A. Kreyssig, S. Nandi, M. G. Kim, A. Thaler, N. Ni, P. C. Canfield, R. J. McQueeney, J. Schmalian, and A. I. Goldman, Phys. Rev. B **81**, 140501(R) (2010).

[21] W. Z. Hu, J. Dong, G. Li, Z. Li, P. Zheng, G. F. Chen, J. L. Luo, and N. L. Wang, Phys. Rev. Lett. **101**, 257005 (2008).

[22] R. M. Fernandes and J. Schmalian, Phys. Rev. B **82**, 014520 (2010).

[23] D. J. Singh and M.-H. Du, Phys. Rev. Lett. **100**, 237003 (2008).

[24] V. Cvetkovic and Z. Tesanovic, EPL **85**, 37002 (2009).

[25] M. M. Korshunov and I. Eremin, Phys. Rev. B **78**, 140509(R) (2008).

[26] P. M. R. Brydon and C. Timm, Phys. Rev. B **80**, 174401 (2009).

[27] I. Eremin and A. V. Chubukov, Phys. Rev. B **81**, 024511 (2010).

[28] W. Baltensperger and S. Strassler, Phys. Kondens. Mater. **1**, 20 (1963).

[29] L. N. Bulaevskii, A. I. Rusinov, and M. Kulic, J. Low Temp. Phys. **39**, 255 (1980).

[30] M. J. Nass, K. Levin, and G. S. Grest, Phys. Rev. Lett. **46**, 614 (1981).

[31] K. Machida, J. Phys. Soc. Jpn. **50**, 2195 (1981).

[32] A. M. Gabovich and A. S. Shpigel, J. Phys. F: Met. Phys. **14**, 3031 (1984).

[33] M. Gulácsi and Zs. Gulácsi, Phys. Rev. B **33**, 6147 (1986).

[34] M. Kato and K. Machida, Phys. Rev. B **37**, 1510 (1988).

[35] M. L. Kulić, E. Goreatchkovski, A. I. Lichtenstein, and M. Mehring, Physica C **252**, 27 (1995).

[36] W. A. Atkinson, Phys. Rev. B **75**, 024510 (2007).

[37] T. Das, R. S. Markiewicz, and A. Bansil, Phys. Rev. B **77**, 134516 (2008).

[38] A. B. Vorontsov, M. G. Vavilov, and A. V. Chubukov, Phys. Rev. B **79**, 060508(R) (2009).

[39] V. Stanev, J. Kang, and Z. Tesanovic, Phys. Rev. B **78**, 184509 (2008).

[40] D. Parker, M. G. Vavilov, A. V. Chubukov, and I. I. Mazin, Phys. Rev. B **80**, 100508(R) (2009).

[41] M. G. Vavilov, A. V. Chubukov, and A. B. Vorontsov, Supercond. Sci. Technol. **23**, 054011 (2010).

[42] A. B. Vorontsov, M. G. Vavilov, and A. V. Chubukov, Phys. Rev. B **81**, 174538 (2010).

[43] P. Ghaemi and A. Vishwanath, arXiv:1002.4638 (unpublished).

[44] I. I. Mazin, D. J. Singh, M. D. Johannes, and M. H. Du, Phys. Rev. Lett. **101**, 057003 (2008).

[45] K. Kuroki, S. Onari, R. Arita, H. Usui, Y. Tanaka, H. Kontani, and H. Aoki, Phys. Rev. Lett. **101**, 087004 (2008).

[46] A. V. Chubukov, D. V. Efremov, and I. Eremin, Phys. Rev. B **78**, 134512 (2008).

[47] H. Ikeda, J. Phys. Soc. Jpn. **77**, 123707 (2008).

[48] F. Wang, H. Zhai, Y. Ran, A. Vishwanath, and D.-H. Lee, Phys. Rev. Lett. **102**, 047005 (2009).

[49] R. Sknepnek, G. Samolyuk, Y. B. Lee, and J. Schmalian, Phys. Rev. B **79**, 054511 (2009).

[50] S. Graser, T. A. Maier, P. J. Hirschfeld, and D. J. Scalapino, New J. Phys. **11**, 025016 (2009).

[51] J. Zhang, R. Sknepnek, R. M. Fernandes, and J. Schmalian, Phys. Rev. B **79**, 220502(R) (2009).

[52] I. I. Mazin and J. Schmalian, Physica C **469**, 614 (2009).

[53] C. Liu, T. Kondo, R. M. Fernandes, A. D. Palczewski, E. D. Mun, N. Ni, A. N. Thaler, A. Bostwick, E. Rotenberg, J. Schmalian, S. L. Bud'ko, P. C. Canfield, and A. Kaminski, Nat. Phys. **6**, 419 (2010).

[54] D. J. Van Harlingen, Rev. Mod. Phys. **67**, 515 (1995).

[55] C. C. Tsuei and J. R. Kirtley, Rev. Mod. Phys. **72**, 969 (2000).

[56] C.-T. Chen, C. C. Tsuei, M. B. Ketchen, Z.-A. Ren, and Z. X. Zhao, Nat. Phys. **6**, 260 (2010).

[57] Y. Sekiba, T. Sato, K. Nakayama, K. Terashima, P. Richard, J. H. Bowen, H. Ding, Y.-M. Xu, L. J. Li, G. H. Cao, Z.-A. Xu, and T. Takahashi, New J. Phys. **11**, 025020 (2009).

[58] V. Brouet, M. Marsi, B. Mansart, A. Nicolaou, A. Taleb-Ibrahimi, P. Le Fevre, F. Bertran, F. Rullier-Albenque, A. Forget, and D. Colson, Phys. Rev. B **80**, 165115 (2009).

[59] C. Liu, A. D. Palczewski, T. Kondo, A. N. Thaler, N. Ni, S. L. Bud'ko, P. C. Canfield, and A. Kaminski (unpublished).

[60] Notice that this quantity is a factor of 2 greater than the g, we defined in our previous work, Ref. 20.

[61] J. M. Kosterlitz, D. R. Nelson, and M. E. Fisher, Phys. Rev. B **13**, 412 (1976).

[62] A. Aharony, J. Stat. Phys. **110**, 659 (2003).

[63] A. Kreyssig, M. G. Kim, S. Nandi, D. K. Pratt, W. Tian, J. L. Zarestky, N. Ni, A. Thaler, S. L. Bud'ko, P. C. Canfield, R. J. McQueeney, and A. I. Goldman, Phys. Rev. B **81**, 134512 (2010).

[64] S.-C. Zhang, Science **275**, 1089 (1997).

[65] E. Demler, W. Hanke, and S.-C. Zhang, Rev. Mod. Phys. **76**, 909 (2004).

[66] D. Podolsky, H.-Y. Kee, and Y. B. Kim, EPL **88**, 17004 (2009).

[67] L. V. Keldysh and Y. V. Kopaev, Fiz. Tverd. Tela **6**, 2791 (1964) [Sov. Phys. Solid State **6**, 2219 (1965)].

[68] J. Des Cloizeaux, J. Phys. Chem. Solids **26**, 259 (1965).
[69] P. C. Canfield and G. W. Crabtree, Phys. Today **56** (3), 34 (2003).
[70] P. Hohenberg, Phys. Rev. **158**, 383 (1967); N. D. Mermin and H. Wagner, Phys. Rev. Lett. **17**, 1133 (1966).
[71] D. Parker and I. I. Mazin, Phys. Rev. Lett. **102**, 227007 (2009).
[72] J. Wu and P. Phillips, Phys. Rev. B **79**, 092502 (2009).
[73] J. Linder, I. B. Sperstad, and A. Sudbø, Phys. Rev. B **80**, 020503(R) (2009).
[74] A. V. Chubukov, Physica C **469**, 640 (2009).
[75] A. V. Chubukov, M. G. Vavilov, and A. B. Vorontsov, Phys. Rev. B **80**, 140515(R) (2009).
[76] R. Thomale, C. Platt, J. Hu, C. Honerkamp, and B. A. Bernevig, Phys. Rev. B **80**, 180505(R) (2009).
[77] P. Bonville, F. Rullier-Albenque, D. Colson, and A. Forget, EPL **89**, 67008 (2010).
[78] T. M. Rice, Phys. Rev. B **2**, 3619 (1970).
[79] Y. Zhang, E. Demler, and S. Sachdev, Phys. Rev. B **66**, 094501 (2002).
[80] C. Fang, H. Yao, W.-F. Tsai, J. P. Hu, and S. A. Kivelson, Phys. Rev. B **77**, 224509 (2008).
[81] C. Xu, M. Müller, and S. Sachdev, Phys. Rev. B **78**, 020501(R) (2008).
[82] R. M. Fernandes, L. H. VanBebber, S. Bhattacharya, P. Chandra, V. Keppens, D. Mandrus, M. A. McGuire, B. C. Sales, A. Sefat, and J. Schmalian, arXiv:0911.3084 (unpublished).
[83] For a recent review, see G. Knebel, D. Aoki, and J. Flouquet, arXiv:0911.5223, Kotai Butsuri (to be published).
[84] E. D. Isaacs, P. Zschack, C. L. Broholm, C. Burns, G. Aeppli, A. P. Ramirez, T. T. M. Palstra, R. W. Erwin, N. Stücheli, and E. Bucher, Phys. Rev. Lett. **75**, 1178 (1995).
[85] S. Sachdev, arXiv:1002.3823 (unpublished).
[86] S. Sachdev, *Quantum Phase Transitions* (Cambridge University Press, Cambridge, England, 2001).
[87] P. C. Canfield, P. L. Gammel, and D. J. Bishop, Phys. Today **51** (10), 40 (1998).
[88] For a review, see in *Superconductivity in Ternary Compounds*, edited by M. B. Maple and Ø. Fisher (Springer-Verlag, Berlin, 1982), Vol. II.
[89] P. Coleman, in *Handbook of Magnetism and Advanced Magnetic Materials*, edited by H. Kronmuller and S. Parkin (Wiley, New York, 2007), Vol. 1, p. 95.
[90] M. Rotter, M. Tegel, I. Schellenberg, F. M. Schappacher, R. Pöttgen, J. Deisenhofer, A. Günther, F. Schrettle, A. Loidl, and D. Johrendt, New J. Phys. **11**, 025014 (2009).
[91] Y. Kamihara, T. Nomura, M. Hirano, J. E. Kim, K. Kato, M. Takata, Y. Kobayashi, S. Kitao, S. Higashitaniguchi, Y. Yoda, M. Seto, and H. Hosono, New J. Phys. **12**, 033005 (2010).
[92] R. T. Gordon, N. Ni, C. Martin, M. A. Tanatar, M. D. Vannette, H. Kim, G. D. Samolyuk, J. Schmalian, S. Nandi, A. Kreyssig, A. I. Goldman, J. Q. Yan, S. L. Bud'ko, P. C. Canfield, and R. Prozorov, Phys. Rev. Lett. **102**, 127004 (2009).
[93] S. Nandi, M. G. Kim, A. Kreyssig, R. M. Fernandes, D. K. Pratt, A. Thaler, N. Ni, S. L. Bud'ko, P. C. Canfield, J. Schmalian, R. J. McQueeney, and A. I. Goldman, Phys. Rev. Lett. **104**, 057006 (2010).